A NOVEL IMAGE SEGMENTATION METHOD IN BREAST ULTRASOUND IMAGES

by

Md. Sayed Ar Rafi (142403)
Nafis Sadik Hossain Anik (142431)
Md. Samiul Alam Toru (142432)
Zahid Hossain (142429)

A Thesis Submitted to the Academic Faculty in Partial Fulfillment of the Requirements for the Degree of

BACHELOR OF SCIENCE IN ELECTRICAL AND ELECTRONIC ENGINEERING

Department of Electrical and Electronic Engineering
Islamic University of Technology (IUT)
Gazipur, Bangladesh

November 2018

A NOVEL IMAGE SEGMENTATION METHOD IN BREAST ULTRASOUND IMAGES

We hereby declare that this thesis has been prepared in partial fulfillment of the requirement for the degree of Bachelor of Science in Electrical and Electronic Engineering at the Islamic University of Technology (IUT), Boardbazar,Gazipur-1704 and has not been submitted any other degree.

| --- | --- | --- | --- |
| Sayed Ar Rafi | Nafis Sadik Hossain Anik | Md. Samiul Alam | Zahid Hossain |
| 142403 | 142431 | 142432 | 142429 |

Approved by:

Md.Taslim Reza

Supervisor, Assistant Processor,
Department of Electrical and Electronic Engineering,
Islamic University of Technology (IUT)
Boardbazar, Gazipur-1704.

Date: .....

Dr. Md. Ashraful Haque

Professor, Head of the Department,
Department of Electrical and Electronic Engineering,
Islamic University of Technology (IUT),
Boardbazar, Gazipur-1704.

Date: .....

List of Tables

Table **Page**

List of Figures

List of Acronyms

BUS	Breast Ultrasound
FFDM	Full Field Digital Mammography
DMIST	Digital Mammography Imaging Screening Trial
CAD	Computer Aided Diagnosis
DBT	Digital Breast Tomography
PPV	Positive Predictive Value
MRI	Magnetic Resonance Imaging
NPV	Negative Predictive Value
BRCA	Breast Cancer gene
PET	Positron Emission Tomography
FDG	2-fluoro 2-deoxy-D-glucose
SONAR	Sound Navigation And Ranging
TM	Time Motion
DEHS	Dynamic Elastography with Harmonic Stimuli
DETS	Dynamic Elastography with Transient Stimuli
ARF	Acoustic Radiation Force
ROI	Region Of Interest
VA	Vibro Acoustography
HMI	Harmonic Motion Imaging
SDUV	Shear Wave Dispersion Ultrasound Vibrometry
TE	Transient Elastography
SWEI	Shear Wave Elasticity Imaging
SSI	Supersonic Shear Imaging
CUSE	Comb-push Ultrasound Shear Elastography
GWE	Guided Wave Elastography
DEXA	Dual Energy X-ray Absorptiometry
DAF	Direction Average Filters
SMSE	Signal to Mean Square Error

NCI	National Cancer Institute
CLAHE	Contrast Limited Adaptive Histogram Equalization
NLM	Neutrosophic l-mean

Contents

Acknowledgements

First of all, we are greatly thankful to the Great Almighty ALLAH who has given us the capability to do all the works. Also, we would like to express our sincere appreciation and gratitude to our advisor, Md. Taslim Reza. Without his consistent and patient academic guidance, we would never have been able to finish this dissertation. His encouragement and career guidance have also been very important for us. His direction is very helpful for us. We are very grateful to our adviser for his contributions, suggestions, moral support and encouragement.

We like to thank our friends who assisted us during our research. Our sincere appreciation goes to our respected elder bothers who helped us during our thesis.

Abstract

Breast cancer is the most commonly diagnosed cancer among women in today's world. In 2017, it's estimated that about 30% of newly diagnosed cancers in women will be breast cancers in the upcoming future. Breast cancer death rates are higher than those for any other cancer, besides lung cancer. Tissue stiffness is related with breast cancer. In case of breast cancer, the tissues become stiffer than normal condition, thus begets malignancy is breast cells. In our work, we use this stiffness to differentiate between benign and malignant lesions. The malignant tissues are stiffer than the benign tissues. Generally, malignant tissues are considered to be cancerous cell. In early days, manual palpation was used to find the breast tumor. But this method lacks effectiveness and accuracy because of its dependence on physician experience. To obtain more effectiveness and accuracy, an imaging method is proposed. Ultrasonography was introduced in the early 90's in order to examine the stiffness of the body cells based on the elasticity of pre-compressed and post-compressed tissues. This imaging method comes along with a great accuracy because of its independence from physician experience. Even though ultrasonography is very useful; because of its low contrast of imaging and speckle noise, a fully automatic segmentation is still a very difficult task. In our research, we try to create a fully automatic lesion segmentation.

In our proposed method, using contrast property of BUS (B-mode Ultrasound) image, we generate a fully automatic ROI (region of interest). Then, we use "Canny filter" to convert the greyscale image to binary image. Thereafter, we count the white pixel from the generated ROI and based on the priority of the counted white pixel, we use ranking to select the best group of images. After that, we use watershed-based technique to improve the group of images even further. Then, we use cross-correlation techniques to co-relate the other images with the best image. So that, we can get better position of lesion than the conventional manual palpation method with greater accuracy.

In our study, cases with multiple-lesions and severe shadowing effect (shadow areas which show similar intensity as the lesions of interest) are omitted.

Chapter 1

Introduction

Breast cancer is the most commonly occurring cancer in women and the second most common cancer overall. In 2012, it represented about 12 percent of all new cancer cases and 25 percent of all cancers in women. Nearly 1.7 million new breast cancer cases were diagnosed in 2012. Breast cancer is the most frequently diagnosed cancer among women in 140 of 184 countries worldwide and now represents one in four of all cancers in women [2]. The most important strategy to survive breast cancer is to detect its presence at primitive stage. Early detection results in not only avoiding unnecessary tests and saving time but also ensuring the medical assistance of more terminal patients. Newer diagnostic techniques in imaging, tissue diagnosis and cytobiological assessments are being developed, which promise to improve early detection and identify women at potentially high risk of the disease. Mammography has been the golden standard for screening for breast cancer, but it has limitations, particularly in younger women and dense breasts. Newer and more specific screening and diagnostic tests are required for early detection of breast cancer, especially in high-risk groups [3]. The earlier the cancers are detected, the better the treatment that can be provided. Early detection requires an accurate and reliable diagnosis which should also be able to distinguish between benign and malignant tumors. Further, a good detection approach should produce both a low false positive rate and a false negative rate [4].

1.1 Mamography

The beneficial effects on cause-specific survival of screening mammography in women aged 50-60 years has been shown in all studies that compared screening with no screening for breast cancer. A study of all such trials showed a reduction in mortality of 20-30% [5]. For women in their 40s, 15-year mortality from breast cancer was reduced by 20% [6], even though mammographic screening has been shown it to be most effective after 55 years of age [7]. The accuracy of conventional analog mammography is influenced by age and breast

density, with sensitivity in dense breasts as low as 30–48% [8]. Sensitivity increases from 69% at 40 years of age to 83% at 75 years [9]. On average, 11% of women undergoing mammography screening need further diagnostic workup, of which 3% turn out to have a malignancy [10]. False-positive mammography increases the anxiety of patients [11]. Young age, dense breasts, use of estrogen-replacement therapy, family history of breast cancer and increased interval between mammography are some of the factors leading to false-positive mammography [12]. A poorer sensitivity of mammography in young women with dense breasts can also lead to false-negative interpretations of the mammography [13]. Thus, advancement in conventional mammography may bring us to improved early detection. But disadvantages of mammography screening lie in radiation risks, risk of false alarm, interval cancers, overdiagnosis and other risks.

1.1.1 Full-Field Digital Mammography

Full-field digital mammography (FFDM) utilizes digital detectors in place of the screen and film used in conventional mammography, giving more latitude and contrast resolution [69].

Digital detectors absorb x-ray photons and convert them into electric charge, and with the help of analog- to-digital converters, the image is changed to digital value (Figures A & B) [70].

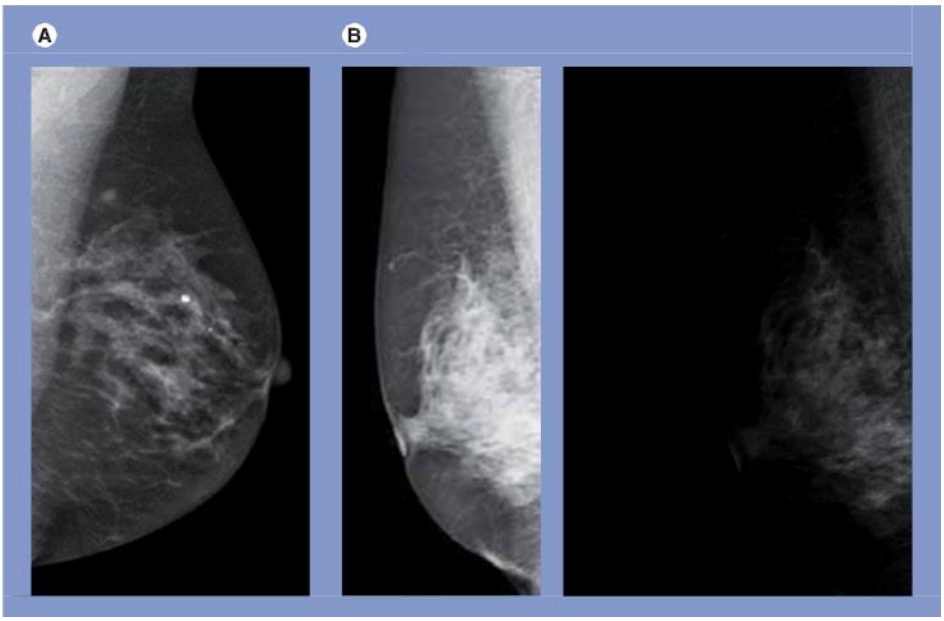

Figure 1.1: Full-Field Digital Mammography

Full-field digital mammography optimizes image acquisition, storage and display, as well as allowing manipulation of image-contrast postprocessing. A multicenter FFDM trial showed sensitivity of 70% compared with 55% for conventional mammograms in women with dense breasts and aged under 50 years [71]. The DMIST was designed to measure small but potentially important clinical differences in diagnostic accuracy between digital and film mammogram. This was a multicentric trial, which recruited almost 50,000 women. All of the participants underwent both digital and film screening mammography in random order. In total, 85.8% had negative FFDM and mammography, 5.7% had positive mammography, 5.6% had positive FFDM and 2.9% had positive FFDM and mammography. The performance of digital mammography was no different than film-screen mammography as a whole, but was significantly better than film-screen mammography among women aged under 50 years (i.e., premenopausal, perimenopausal and women with dense breasts). FFDM also pro- vided easier access to images and use of computer-aided detection (CAD), and easier storage and retrieval of images. The use of FFDM may be justified in the specific subgroup where it showed increased sensitivity. Fischmann conducted a study in 200 women to compare image quality

and lesion detection for FFDM and conventional full-screen mammography [72]. No improvement in detection of masses with FFDM was reported, but FFDM was advantageous owing to its contrast resolution in excluding masses and better classified parenchymal density. There was also better depiction of nipple, skin and pectoral muscle. The paper concluded that FFDM was equal or superior to conventional mammography for all image quality and detection parameters studied.

A prospective study carried out to compare FFDM with conventional mammography for detection and characterization of micro-calcifications found that the image quality of FFDM was superior in over 50% of cases [5]. In total, 40% of cases showed more calcifications in the FFDM arm, and FFDM had a sensitivity of 95.2% and specificity of 39.3% compared with 91.9 and 36.3% for conventional mammography [5]. Higher diagnostic accuracy was shown in FFDM. Other advantages are constant image exposure at an optimal level and less need for repeat imaging, no film artifacts, and the ability to allow almost instant data transfer between centers. Although Lewin et al. found no significant difference in cancer detection between FFDM and conventional mammography in a screening population, FFDM did result in fewer recall rates [73]. FFDM use is rapidly expanding in clinical settings and the outcome of this rapid uptake is currently being investigated in various studies.

1.1.2 Contrast-Enhanced Mammography

There are two basic techniques that use contrast in imaging breast: temporal-subtraction mammography and dual-energy mammography. For temporal-subtraction mammography, an unenhanced image is obtained, followed by a contrast-enhanced image [74,75]. As in contrast- enhanced MRI, pre-contrast images are subtracted from postcontrast images for evaluation of enhancement. This technique is based on MRI protocols where malignant tumors show an atypical washout pattern, though it cannot adopt the pattern obtained by MRI [76]. The major draw- back is the presence of motion artifacts and the higher radiation dose to patients.

Dual-energy mammography is another method of visualizing contrast in mammography systems. After giving intravenous contrast, two images of breast are obtained, one with a higher energy level, which absorbs more x-rays. The two images are then subtracted for

optimal visualization of the contrast. This technique utilizes much more energy levels as compared with conventional imaging [77]. For visualization of contrast agents in the dual-energy mode, slot-scan mammography systems with detectors using narrow x-ray beam to scan the breast can be used. In addition, photon-counting system detectors, which can distinguish photons with high energy from those with low energy levels within a single image, are available.

This technique is still developing and its status within the available imaging techniques is still not defined. There also seems to be debate on whether iodine is the appropriate contrast medium for breast, as the low-energy-level radiation used in mammograms may not give optimal visualization with iodine.

1.1.3 Tomosynthesis

Breast tomosynthesis is an advanced form of mammography, a specific type of breast imaging that uses low-dose x-rays to detect cancer early when it is most treatable. Breast tomosynthesis is not yet available in all imaging facilities [23]. DBT, first described by Niklason and colleagues [24] in 1997, reconstructs a tomographic quasi-three-dimensional (3D) radiographic image of the breast by applying a mathematical algorithm to a few low-dose 2D projection images. Reconstructed 3D images are superior to 2D mammograms mainly because they provide blurring of the tissue above and below the selected plane lowering the effect of overlapping breast tissue. A composite 2D image, which looks like a conventional FFDM image, can also be generated from the projection images, the so-called synthetic view. In DBT, the breast is compressed against a detector while the x-ray tube rotates around the breast in an arc and captures a series of 2D images that are known as projections [25,26].

1.2 Computer-Aided Diagnosis

Computer-aided detection programs recognize abnormal patterns in breast imaging and draw attention to masses, calcifications and parenchymal asymmetry on the digital breast image [14]. CAD is helpful in reducing variability among radiologists [15]. Various studies investigating CAD in screening mammography demonstrate its ability to detect mammographic signs of cancer and reduce the false-negative rate by 50–70% [16]. In some studies, CAD missed findings [17], but there are also concerns that CAD may unduly increase

recall rate and biopsy rates [18]. CAD resulted in a 19.5% increase in the number of malignancies detected and also improved detection of early breast cancer from 73 to 78% [19]. It appears that CAD increases sensitivity but may lead to a fall in specificity; however, in this study the positive predictive value (PPV) for biopsy was not affected by CAD, and the radiologist and CAD were statistically equal in their ability to detect mammographic signs of malignancy [19]. Another study, conducted to test radiologist performance with use of CAD in breast cancer diagnosis, found that the receiver operator curve increased from 0.61 without CAD to 0.75 with use of CAD. Use of CAD increased the sensitivity (from 73.5 to 87.4%) and specificity (from 31.6 to 41.9%) for detection of malignant breast lesions [20]. Fenton et al. studied the association between use of CAD at mammography facilities and performance of screening mammography. They found that diagnostic specificity reduced from 90.2% before implementation of CAD to 87.2% after its introduction. The rate of breast biopsy increased by 19.7%, and an increase in sensitivity from 80.4 to 84.0% was not found to be statistically significant. This study concluded that use of CAD is associated with reduced accuracy of interpretation of screening mammography [21].

The current CAD system is not for independent use but may act as an adjunct to radiological interpretation. CAD can also be used with FFDM to improve interpretation of results [21]. The

most popular CAD system currently used is the R2 image checker, which marks potential breast masses, microcalcifications and lesions with high probability of malignancy [22].

1.3 Magnetic Resonance Imaging

Dynamic contrast-enhanced MRI mammography is a technique that has been widely studied over the last decade, particularly as a screening modality for young women with a high risk for familial breast cancer and women with dense breasts. Its use as an adjunct to routine screening imaging to clarify inconclusive or suspicious findings is gaining popularity, and to more accurately size tumors where clinical and mammogram or ultra- sonography breast findings have disparity. The overall NPV for breast MRI is 84.5% [78]. It has a high PPV and high NPV to differentiate surgical scarring from recurrence [79,80]. The largest body of evidence to date is its value in screening high-risk younger women. Multiple prospective studies have evaluated the role of MRI in high-risk patients, and concluded that diagnosis of breast cancer in this group is improved by use of MRI, with a sensitivity of 79–98% [81]. The American Cancer Society guidelines recommend that MRI and mammography should be used for annual screening of all women who have a BRCA mutation or lifetime risk of 20–25% or more [82].

MRI is also used to look for breast malignancy in patients with an unknown primary who have negative conventional breast imaging [83], and in patients with locally advanced breast cancer undergoing neo-adjuvant treatment, where MRI can be used to identify responders: the earliest sign of response is change of enhancement kinetics, which precedes change in tumor morphology by weeks [84]. It is also useful to detect residual disease burden after completion of chemotherapy [85]. It is also the method of choice to detect local recurrence of breast cancer and to estimate residual malignancy in the breast after wide local excision where margins of resection are considered inadequate [86].

Patients with breast implants always pose a challenge for imaging, and MRI can delineate cancer obscured by the implant. MRI is also the method of choice in the evaluation of the augmented breast, with very high accuracy in assessment of implant integrity and in cancer detection [87].

1.4 PET-Scan

PET-scan utilizes (18F)2-fluoro-2-deoxy-D- glucose (FDG), a substrate that is rapidly utilized by malignant cells that display a higher metabolic rate as compared with normal tissues. Thus, malignant cells show increased uptake of FDG on PET scan [88].

PET is limited by its inability to detect lesions smaller than 1 cm, although it is not affected by breast density, previous breast surgery or irradiation to breast. It also has very limited usefulness in detection of ductal carcinoma in situ, lobular cancer and multicentric tumors [89]. PET appears to have no role in the diagnosis of primary breast cancer, although it appears to be promising in detection of distant metastasis and recurrence of breast cancer. It may also be used to monitor response to chemotherapy by evaluating change in tumor size. A complete or partial response to treatment is indicated by reduced FDG uptake on PET as compared with non- responsive breast tumor, where FDG uptake remains unchanged [90]. Some tumors have low uptake, while some inflammatory lesions lead to false-positive results. PET computed tomography allows anatomical localization of the increased tracer uptake seen on PET scan. For primary breast tumor detection, this technique may have a role in dense breasts, breasts with implants and in those patients where mammography is indeterminate and breast biopsy is not a desirable option [91].

It may also be useful in localizing and differentiating between malignant and reactive axillary and internal mammary lymph nodes [92]. One report investigated the role of PET-computed tomography in evaluation of breast cancer, and concluded that its major role is in detecting meta- static disease, tumor recurrence and evaluating response to treatment [93].

1.5 Breast Ultrasonography

Ultrasonography can be used as a supplement to routine screening of young, pregnant and lactating women, women with dense breast tissue on mammography, and those at high risk, targeting an area of concern in the breast. It may detect an additional 3–4 cancers per 1000 women in high-risk groups [27]. More than 90% of cancers seen only on ultrasonography are in dense breasts, of which 94% are invasive [28] and 70% are less than 1 cm in size and are thus clinically impalpable [29].

A combination of negative diagnostic mammogram and negative ultrasonography has a sufficiently high negative predictive value (NPV) that biopsy of a low-suspicion palpable mass is not indicated [30]. On the other hand, PPV of biopsy for lesions seen only on ultrasonography is low, averaging 11% [31].

Ultrasonography is particularly useful to localize and allow biopsy of lesions seen on MRI but not on mammogram. Its role in preoperative staging of the axilla is also being studied. Malignant lymph nodes are identified by loss of fatty hilum and cortical nodularity [32,33].

While breast ultrasonography is painless and requires no radiation, it relies heavily on the operator's experience. To reduce the inconsistencies arising with hand-held transducers, some companies are developing an automated multidetector sweep scanning device that will permit precise localization and correlation in two planes within the breast, and may also allow reconstitution of images in a coronal plane [29,31].

1.5.1 Working Principle of Ultrasound Imaging

Ultrasound or ultrasonography is a medical imaging technique that uses high frequency sound waves and their echoes. The technique is similar to the echolocation used by bats, whales and dolphins, as well as SONAR used by submarines. In ultrasound, the following events happen:

1.The ultrasound machine transmits high-frequency (1 to 5 megahertz) sound pulses into your body using a probe.

2.The sound waves travel into your body and hit a boundary between tissues (e.g. between fluid and soft tissue, soft tissue and bone).

3.Some of the sound waves get reflected back to the probe, while some travel on further until they reach another boundary and get reflected.

4.The reflected waves are picked up by the probe and relayed to the machine.

5.The machine calculates the distance from the probe to the tissue or organ (boundaries) using the speed of sound in tissue (5,005 ft/s or1,540 m/s) and the time of each echo's return (usually on the order of millionths of a second).

6.The machine displays the distances and intensities of the echoes on the screen, forming a two-dimensional image.

A basic ultrasound machine has the following parts:

i.Transducer probe - probe that sends and receives the sound waves

ii.Central processing unit (CPU) - computer that does all of the calculations and contains the electrical power supplies for itself and the transducer probe

iii.Transducer pulse controls - changes the amplitude, frequency and duration of the pulses emitted from the transducer probe

iv.Display - displays the image from the ultrasound data processed by the CPU

v.Keyboard/cursor - inputs data and takes measurements from the display

vi.Disk storage device (hard, floppy, CD) - stores the acquired images

vii.Printer - prints the image from the displayed data

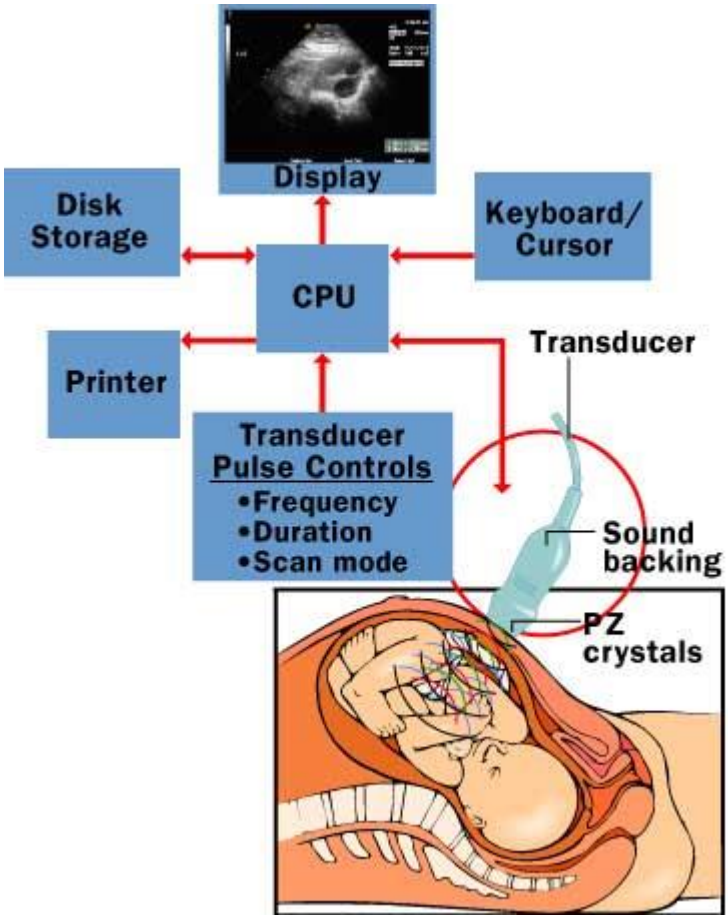

Figure 1.2: The Parts of Ultrasound Machine [34]

1.5.2 Ultrasound Scanning Modes

Typically, there are three types of ultrasound scanning modes available. They are:

A-Mode: A-Mode (Amplitude Mode) is the display of amplitude spikes of different heights. This mode is considered 1D and used to measure the distance between two objects by dividing the speed of sound by half of the measured time between the peaks in the A-mode plot, which represents the two objects in question. A-Mode consists of a x and y axis, where x represents the depth and y represents the Amplitude.

B-Mode: B-Mode (Brightness Modulation) is the display of 2D map of B-Mode data, and is the most common form of ultrasound imaging. Unlike A-Mode, B-Mode is based on brightness with the absence of vertical spikes. Therefore, the brightness depends upon the amplitude or intensity of the echo. There is no y axis on B-Mode, instead, there is a z axis, which represents

the echo intensity or amplitude, and a x axis, which represents depth. B-Mode will display an image of large and small dots, which represent strong and weak echoes, respectively.

M-Mode: M-Mode (Motion Mode) is the display of a one-dimensional image that is used for analyzing moving body parts commonly in cardiac and fetal cardiac imaging. It is also called Time Motion or TM-Mode. This can be accomplished by recording the amplitude and rate of motion in real time by repeatedly measuring the distance of the object from the single transducer at a given moment. The single sound beam is transmitted and the reflected echoes are displayed as dots of varying intensities thus creating lines across the screen.

There are some other types of scanning modes: -
C-Mode: A C-mode image is formed in a plane normal to a B-mode image. A gate that selects data from a specific depth from an A-mode line is used; then the transducer is moved in the 2D plane to sample the entire region at this fixed depth. When the transducer traverses the area in a spiral, an area of 100 cm2 can be scanned in around 10 seconds.

Doppler Mode:

This mode makes use of the Doppler effect in measuring and visualizing blood flow.
Color Doppler: Velocity information is presented as a color-coded overlay on top of a B-mode image.

Continuous wave (CW) Doppler: Doppler information is sampled along a line through the body, and all velocities detected at each time point are presented (on a time line).

Pulsed wave (PW) Doppler: Doppler information is sampled from only a small sample volume (defined in 2D image), and presented on a timeline

Duplex: A common name for the simultaneous presentation of 2D and (usually) PW Doppler information. (Using modern ultrasound machines, color Doppler is almost always also used; hence the alternative name Triplex).

Pulse Inversion Mode:

In this mode, two successive pulses with opposite sign are emitted and then subtracted from each other. This implies that any linearly responding constituent will disappear while gases with non-linear compressibility stand out.

Harmonic Mode:

In this mode, a deep penetrating fundamental frequency is emitted into the body and a harmonic overtone is detected. This way noise and artifacts due to reverberation and aberration are greatly reduced. Some also believe that penetration depth can be gained with improved lateral resolution; however, this is not well documented.

1.5.3 Ultrasound Based Elastography Methods

Ultrasound imaging is a low-cost, safe and mobile imaging modality that can generate real-time images and has found broad applications in clinical radiology. Safety is one of its major strengths; indeed, this technique does not involve ionizing radiations. Ultrasound-based elastography methods use ultrasound imaging to track the deformation behavior of soft tissues and further infer the elastic properties of both healthy and diseased soft tissues. Depending on the features of the stimuli used to deform the soft tissue, the ultrasound-based elastography methods can be divided into three categories: static elastography, DEHS and DETS. This section gives an overview of different ultrasound-based elastography techniques and their applications for the mechanical characterization of soft tissues and diagnosis of some diseases.

Static Elastography Methods: Static elastography, which was proposed in the early 1990s, has been widely used in clinics in the past two decades [94-101]. When using this method, static compression is typically imposed onto a targeted soft tissue. The resulting displacement field (mainly the axial displacement in the early use of static elastography) generated by the compressive load can be directly measured via the ultrasound imaging method. The strain field can then be calculated according to the measured displacement. Furthermore, dedicated inverse approaches can be used to extract the elastic properties of the target soft tissues according to the strain field [94,98,102,103]. Briefly, harder tissues have lower strains, whereas softer tissues have higher strains under compression. In principle, it is possible to quantitatively infer the elastic properties of soft tissues using a static elastography method; however, this is challenging because of the complexity of the associated inverse problem. Therefore, the static elastography method is usually regarded as a qualitative method that reveals the contrast between hard and soft tissues.

Although the limitations of the static elastography method in quantitatively measuring the mechanical properties of soft tissues have been recognized, this method is simple and easy

to realize and allows us at least to qualitatively distinguish between regions with different stiffnesses; therefore, it has been widely used in clinics.

Dynamic Elastography with Harmonic Stimuli:

DEHS are elastography techniques that use external or internal harmonic stimuli to generate dynamic responses in biological soft tissues. Here, we focus on cases in which external vibrators or ARFs generated by focused ultrasound beams are used as stimuli.

Sonoelastography: The sonoelastography imaging method uses an external harmonic vibrator to generate harmonic vibrations within target soft tissues [94,98]. The steady-state responses (e.g. the map of the vibration amplitude and phase) of the tissues are then measured using the Doppler spectrum of the reflected signals [104,105]. Accordingly, different inverse approaches are established to obtain the elastogram of the tissues. Based on the distribution of the vibration amplitude, local lesions, which may be harder or softer than surrounding tissues, can be distinguished [106].

Shear wave-induced resonance elastography: A recently developed method named SWIRE adopts an external vibrator to generate shear waves with frequencies in the range of 45–205 Hz within soft materials. The propagation of the shear waves is monitored by an ultrafast ultrasound scanner. Then, Fourier transformation is conducted for the time-domain displacement at each point in the region- of-interest (ROI) to obtain the frequency-domain displacement. Additionally, a finite-element (FE) model is used to simulate the experiments and calculate the theoretical resonance frequencies of soft inclusions with different elastic parameters. When the theoretical results match the experimental ones, the corresponding elastic parameters are supposed to be those of the practical soft inclusion.

Vibro-acoustography: In the VA technique [107-109], confocal transducers with center frequencies $\omega 1$ and $\omega 2$ are applied to a target soft material. $\omega 1$ and $\omega 2$ are on the order of megahertz, whereas $\delta\omega = \omega 2 - \omega 1$ is on the order of kilohertz. Thus, the low-frequency (kHz) harmonic ARF can be imposed onto a focused point within the target soft tissue [107]. The resulting vibration, which is determined by the local elastic properties of the tissue at the focused point, will induce an acoustic emission field. Both the magnitude and phase of the acoustic emission can be detected by a hydrophone. When the two focused ultrasound beams

sweep through the whole object, images based on either the magnitude or phase of the acoustic emission can be obtained

Harmonic motion imaging:

In the HMI method, an additional ultrasound beam is used to monitor the harmonic motion induced by confocal transducers. The amplitude of the harmonic motion of soft tissues is determined by both the local elastic properties at the focus and the magnitude of the ARF.

Shear wave dispersion ultrasound vibrometry:

The SDUV technique, which was developed by Chen et al. [110,111], uses the harmonic ARF generated by an amplitude-modulated ultrasound beam to induce low-frequency shear waves (typically ranging from 300 to 900 Hz) within target soft tissues. The shear waves are detected at different locations along the propagation direction, and then the phase velocities can be determined via the phase gradient method. For a viscoelastic solid, the phase velocities depend on the frequencies of the shear waves, and the relationship between the phase velocities and the frequencies is the so-called dispersion relation. By controlling the modulation frequency, the frequency of the generated shear wave can approximately vary from 300 to 900 Hz and the dispersion curve can be obtained.

Dynamic Elastography with Transient Stimuli: In DETS methods, the responses of soft tissues (e.g. the shear wave velocities) are measured to extract the local elastic properties [17,18,20,94–98]. Note that in this method, the frame rate of the scanner is usually high enough to acquire the propagation process of the shear waves. A key merit of DETS is that it is not so sensitive to the BCs. The reflected waves are separated from the incident wave in the time domain and can be filtered out [17]. Therefore, DETS enables the quantitative determination of elastic properties. Similar to DEHS, various external and internal stimuli may be used to generate transient shear waves within soft tissues. In recent years, DETS, in which the ARF is used to generate a transient shear wave, has attracted considerable attention [4,7,18,20,95,96,99,100]. This method, which generates remotely transient shear waves within biological tissues, permits us to probe the mechanical properties of biological tissues and is relatively suitable for clinical use.

Transient elastography: Transient elastography (TE), which was proposed by Sandrin and colleagues [112,113], uses an external vibrator to introduce a low-frequency transient wave in biological tissues and tracks the propagation of this transient wave along the axis of the

vibrator, with a frame rate of approximately 4000 Hz. The velocity of the transient wave is measured, and the elastic modulus of the soft tissue can be quantitatively determined by assuming that the tested material is elastic and its dimension is larger than the wavelength.

Shear wave elasticity imaging and ARF impulse: Sarvazyan et al. [18] proposed the shear wave elasticity imaging (SWEI) method, which uses the ARF to generate shear waves within soft tissues. The magnitude of the ARF is fairly small, and, thus, the displacement induced by the acoustic force within the soft biological tissue is usually on the order of micrometer. However, Sarvazyan et al. [114] demonstrated that using an additional system (e.g. MRI or optical imaging) facilitates recording the shear waves. Subsequently, Nightingale et al. [115] and Palmeri et al. [116] used ultrasound imaging to track the propagation of shear waves in in vivo and ex vivo experiments. AFRI-based SWEI method [115,117,118] is a promising strategy for quantitatively probing the local elastic properties of biological soft tissues. Both generating the ARF and monitoring the propagation of the shear waves can be realized using a single ultrasound probe, unlike in experimental systems that require an extra vibrator to generate shear waves.

Supersonic shear imaging: The supersonic shear imaging (SSI) technique uses ultrasound beams focused at different depths within biological tissues to create a moving ARF [119,120]. The ARF moves at a high speed in the soft material; thus, the resulting displacement field is confined within a Mach cone. In this case, two quasi-plane shear wave-fronts interfere along the Mach cone and propagate in opposite directions. This phenomenon is known as the elastic Cherenkov effect (ECE) [119,121]. In the SSI technique, the propagation of the interfered front is monitored using an ultrafast imaging technique. The fast acquisition reduces the risk of artefacts resulting from the movements of patients or investigators.

Comb-push ultrasound shear elastography: In CUSE method, several unfocused (or focused) ultrasound beams are used as multi-stimuli to generate shear waves in the whole field-of-view (FOV). Additionally, the elastic properties in the whole FOV can be identified with one acquisition. The shear waves are generated by the CUSE in a homogeneous phantom. Both homogeneous and inclusion phantom experiments have been performed to validate the effectiveness of this method. In vivo experiments to detect breast masses and evaluate thyroid nodules have also been conducted, and the results show that this technique is promising [122,123]. In the subsequent study, Song et al. further developed the time-aligned

sequential tracking (TAST) method, which enables the CUSE being realized on traditional ultrasound scanner [124].

Guided wave elastography: The general steps involved in GWE using the ARF as stimuli may be summarized as follows: -

The focused ARF is used to generate the broad-band guided waves in the walls of soft tissues.
The propagation of the guided shear waves is tracked along the propagation direction.
Two-dimensional Fourier transformation can be applied to analyze the spatio-temporal imaging of the guided waves and extract the dispersion relation [125].
A guided wave model. (e.g. the Lamb wave model [126]) can be used to fit the experimental dispersion curve and identify the elastic properties of the thin-walled soft tissues.

1.5.4 Ultrasound Elastography Techniques

From these principles, the different currently available USE techniques can be classified by the measured physical quantity:
Strain imaging: In this technique, a normal stress σ_n is applied to tissue and the normal strain ε_n is measured and an equation 2 is used to provide a qualitative evaluation of Young's modulus E.

Shear wave imaging (SWI): In this technique, a dynamic stress is applied to tissue by using a mechanical vibrating device in 1D transient elastography (1D-TE) or acoustic radiation force in point shear wave elastography (p-SWE) and 2D shear wave elastography (2D-SWE). Shear waves created by the excitation are measured perpendicular to the acoustic radiation force application or parallel to the 1D transient elastography excitation; the shear wave speed cs is reported or Young's modulus E is computed and reported using the following equation:

$$E = 3G = 3\rho c_{s^2}$$

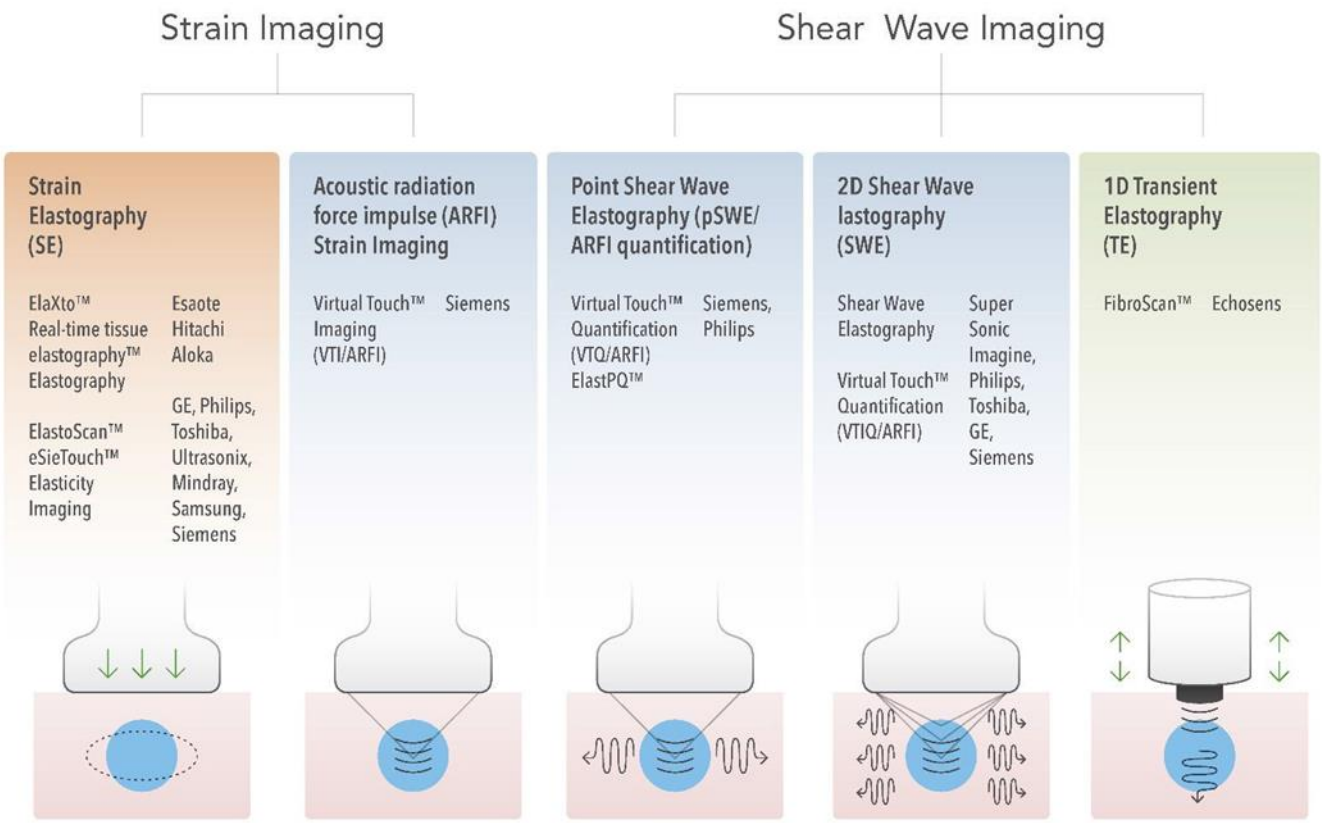

Figure 1.3: Strain and Shear imaging classification

1.5.5 Applications of Ultrasound Imaging

Ultrasound imaging is used in many types of examinations and procedures. Some examples include:

Ultrasounds are useful in the detection of pelvic abnormalities and can involve techniques known as abdominal (trans-abdominal) ultrasound, vaginal (trans-vaginal or endovaginal) ultrasound in women, and also rectal (transrectal) ultrasound in men.

Doppler ultrasound (to visualize blood flow through a blood vessel).

Bone sonography (to diagnose osteoporosis).

Ultrasound can also be used for elastography. This can be useful in medical diagnoses, as elasticity can discern healthy from unhealthy tissue for specific organs/growths.

Echocardiogram (to view the heart).

Fetal ultrasound (to view the fetus in pregnancy).

Ultrasound-guided biopsies.

Doppler fetal heart rate monitors (to listen to the fetal heart beat).

1.5.6 Advantages of Ultrasound Imaging Modality

It is non-ionizing radiation, so it does not have the same risks as x-rays or other types of ionizing radiation.

It images muscle, soft tissue, and bone surfaces very well and is particularly useful for delineating the interfaces between solid and fluid-filled spaces.

It renders "live" images, where the operator can dynamically select the most useful section for diagnosing and documenting changes, often enabling rapid diagnoses. Live images also allow for ultrasound-guided biopsies or injections, which can be cumbersome with other imaging modalities.

It shows the structure of organs.

It has no known long-term side effects and rarely causes any discomfort to the patient.

Equipment is widely available and comparatively flexible.

Small, easily carried scanners are available; examinations can be performed at the bedside.

Relatively inexpensive compared to other modes of investigation, such as computed X-ray tomography, DEXA or magnetic resonance imaging.

Spatial resolution is better in high frequency ultrasound transducers than it is in most other imaging modalities.

Through the use of an Ultrasound research interface, an ultrasound device can offer a relatively inexpensive, real-time, and flexible method for capturing data required for special

research purposes for tissue characterization and development of new image processing techniques.

1.5.7 Limitations of Ultrasound Imaging Modality

Ultrasound imaging devices have trouble penetrating bone. For example, imaging of the adult brain is very limited though improvements are being made in transcranial ultrasonography.

Ultrasound imaging performs very poorly when there is a gas between the transducer and the organ of interest, due to the extreme differences in acoustic impedance. For example, overlying gas in the gastrointestinal tract often makes ultrasound scanning of the pancreas difficult, and lung imaging is not possible (apart from demarcating pleural effusions).

Even in the absence of bone or air, the depth penetration of ultrasound may be limited depending on the frequency of imaging. Consequently, there might be difficulties imaging structures deep in the body, especially in obese patients.

Body habitus has a large influence on image quality, image quality and accuracy of diagnosis is limited with obese patients, overlying subcutaneous fat attenuates the sound beam and a lower frequency transducer is required (with lower resolution)

The method is operator-dependent. A high level of skill and experience is needed to acquire good-quality images and make accurate diagnoses.

There is no scout image as there is with CT and MRI. Once an image has been acquired there is no exact way to tell which part of the body was imaged.

1.6 Lesion Segmentation

Segmentation is an important step of CAD systems. Both automation and accuracy of segmentation is crucial. Automation of segmentation is important because it facilitates the complete automation of the CAD system. A fully automatic CAD can minimize the effect of the operator-dependent nature inherent in ultrasound imaging [35] and make the diagnosis process reproducible. Accuracy of segmentation is important because many crucial features

for discriminating benign and malignant lesions are based on the contour, shape and texture of the lesion (ACR BI-RADS lexicon) [36]. These features can be effectively extracted after the lesion boundary is correctly detected. Thus, an accurate segmentation method is essential for a correct diagnosis. However, there are characteristic artifacts, such as attenuation, speckle, shadows, and signal dropout, which make the segmentation task complicated; these artifacts are due to the orientation dependence of acquisition that can result in missing boundaries. Further complications arise as the contrast between areas of interest is often low [37]. How to do one of the oldest image processing tasks, image segmentation, for breast ultrasound, is a challenging task.

1.6.1 Histogram Thresholding and Region Growing

Simple histogram thresholding [38,39] or region-growing algorithms [40,41] can find the preliminary lesion boundary. In a histogram thresholding method, an intensity threshold is chosen at the valley of the image histogram to separate the image into background and foreground. For a region growing method, a region is grown from the seed point (start point) by adding similar neighboring pixels. Although efficient, these methods cannot generate a precise boundary because their over-simplified concepts and the high sensitivity to noise. However, they can serve as an intermediate step to provide a rough contour [40] or can be combined with post-processing procedures such as morphological operations [38,39,42], disk expansion [43], Bayesian neural network [44], function optimization [45,46] etc. For example, in the thresholding algorithm [38,39], firstly, the regions of interest (ROIs) were preprocessed with a 4×4 median filter to reduce the speckle noise and to enhance the features. Second, a 3×3 unsharp filter was constructed using the negative of a two-dimensional Laplacian filter to emphasize the elements with meaningful signal level and to enhance the contrast between object and background. Third, the ROIs were converted to a binary image by thresholding. The threshold was determined by the histogram of ROIs. If a valley of a histogram between 33% and 66% of the pixel population could be found, this intensity value was selected as the threshold. If there was no such valley in that range, the intensity of 50% of the pixel population was selected as the threshold value. Finally, the selected nodule's boundary pixels were obtained using morphologic operations.

1.6.2 Model-based Methods

Model-based methods have strong noise-resistant abilities and are relatively stable at sonography demarcation. Commonly used models include level set [46-48], active contours [40, 49-52], Markov random fields (MRF) [53-57] etc.

For instance, Sarti et al. [48] discussed a level set maximum likelihood method to achieve a maximum likelihood segmentation of the target. The Rayleigh probability distribution was utilized to model gray level behavior of ultrasound images. A partial differential equation-based flow was derived as the steepest descent of an energy function considering the density probability distribution of the gray levels, as well as smoothness constraints. A level set formulation for the associated flow was derived to search the minimal value of the model. Finally, the image was segmented according to the minimum energy.

Madabhushi and Metaxas [40] combined intensity, texture information, and empirical domain knowledge used by radiologists with an active contour model in an attempt to limit the effects of shadowing and false positives. Their method requires training but in the small database. Using manual delineation of the mass by a radiologist as a reference, and the Hausdorff distance and average distance as boundary error metrics, they showed that their method is independent of the number of training samples, shows good reproducibility with respect to parameters, and gives a true positive area of 74.7%. Some active contour models have been applied to 3-D ultrasound segmentation, such as [49-52].

Boukerroui et al. [53] used a Markov random field to model the region process and to focus on the adaptive characteristics of the algorithm. Their method introduced a function to control the adaptive properties of the segmentation process, and considered both
local and global statistics during the segmentation process. A new formulation of the segmentation problem was utilized to control the effective contribution of each statistical component. The merit of MRF modeling is that it provides a strong exploitation of the pixel correlations. The segmentation results can be further enhanced via the application of maximum a posteriori segmentation estimation scheme based on the Bayesian learning paradigm [37].

In most model-based approaches, an energy function is formulated, and the segmentation problem is transformed as finding the minimum (or maximum) of the energy function iteratively. However, the iterations on calculating energy functions and reformulating the

models are always time-consuming, especially for complex BUS images; and many models are semi-automatic with the requirement of pre-labeled ROI or manually initialized contour.

1.6.3 Machine Learning Method

Machine learning methods (such as neural network and support vector machine) [58-62] are popular in image segmentation, which transform the segmentation problem into a classification decision based on a set of input features. In [61], Dokur and Ölmez proposed a neural network-based segmentation method. Images were divided into square blocks, and features were extracted from each block using the discrete cosine transform (DCT). Then a three-layer hybrid neural network was trained to classify the blocks into two categories: background and foreground. The method was applied on the region of interest (ROI) which needed to be selected by the user. Kotropoulos and Pitas [58] employed a support vector machine with a radial basis function kernel to classify different patterns. In this method, patterns were collected by a running window with size of 15x15 over the entire image. To train the SVM, 1128 positive patterns (lesion) and 1128 negative patterns (background) were selected from the training set. Experiments showed that the trained SVM could generate reasonable segmentation result.

For machine learning methods, feature selection and training process are two key steps that play an important role on segmentation result. If features are sufficiently distinguishable and the method is well trained, machine learning methods can generate satisfactory lesion contours. However, over-training or insufficient training (trapped by local minimum) may severely affect the segmentation performance on new data. And the training process is usually quite time-consuming.

1.6.4 Watershed-Based methods

Watershed-based approaches have shown promising performances for ultrasound image segmentation. The methods consider image as topographic surface wherein the grey level of a pixel is interpreted as its altitude. Water flows along a path to finally reach a local minimum. The biggest challenge for such methods is over-segmentation; to address the problem, many approaches have been proposed and can be categorized into two types: marker-controlled [63-65] and cell competition [66-68].

Marker-controlled methods inundate the gradient landscape of image and define watersheds when the flooding of distinct markers rendezvous with each other. Hence, the identification of makers is very crucial in solving the over-segmentation problem. The method proposed in [63] was a texture-based approach that selected the marker candidates as seeds for the water-level immersion. A self-organization map was trained to identify the texture of lesions as the flooding markers. Distinctively, the method in [64] adopted a thresholding and morphological operation scheme to seek flooding markers. It required a heuristic estimation of the best thresholding of markers to achieve the task of lesion delineation.

Cell competition approaches, on the other hand, alleviate the over-segmentation problem in a different way. A two-pass watershed transformation [66] was performed to generate the cell tessellation on the original ultrasound image or ROI. In this method, a competition scheme based on the cell tessellation was carried out by allowing merge and split operations of cells. The cost function was devised to characterize boundary saliency and regional homogeneity of an image partition, and it drove the competition process to converge to a prominent component structure. However, neither marker-controlled nor cell competition approaches guarantee to solve the over-segmentation problem completely [67].

Table 1.1. Summary of Segmentation Methods for BUS Images.

Methods	Descriptions	Advantages	Disadvantages
Histogram thresholding	Threshold value is selected to segment the image.	Simple and fast.	Only works for bimodal histograms and has no good results for BUS image.
Region growing	Region is grown from the seed point by adding similar neighboring pixels.	The concept is simple. Multiple stop criteria can be chosen.	Seed point is required; sensitive to noise.
Model-based (includes active contour, level set, Markov random field)	A model is used to formulate the lesion contour and the model is revised based on local features such as edges, intensity gradient, texture, and so on.	Robust, self-adapting in search of a minimal energy state.	Time-consuming; pre-labeled ROI or initial contour is required; easy to get stuck in local minima states
Machine learning	Features to separate the lesion from the background are extracted first, and a machine learning method is trained to do the classification based on pixel-level or region-level.	Stable; different lesion characteristics can be incorporated by feature extraction.	Long training time; over-training problem; test images should come from the same platform as the training images.
Watershed (includes marker-controlled watershed and cell competition watershed)	Considers image as topographic surface wherein grey level of a pixel is interpreted as its altitude. Water flows along a path to finally reach a local minimum.	It ensures closed region boundaries.	Over-segmentation problem is not completely solved.

In summary, the major drawbacks of current methods are:

Human interactions such as the pre-labeled ROIs or manually initialized contours are required, which impede full automation

Intensity features are most typically used for boundary detection. Since BUS images have low contrast and are degraded by speckle noise, features based on intensity gradients are always sensitive to noise and cannot guarantee accurate segmentation result

Reformulating the models and training the methods are always time-consuming, especially for complex BUS images. As the image resolution increases, the computational complexity for processing a BUS image also increases.

Chapter 2

SPECKLE REDUCTION

Speckle is an inherent characteristic of ultrasound imaging. It takes the form of multiplicative noise generated by a number of scatterers with a random phase within the resolution cell of an ultrasound beam [128, 129]. The texture of the observed speckle pattern does not correspond to the underlying structure. The local brightness of the speckle pattern, however, does reflect the local echogenicity of the underlying scatterers. There are generally two contrary opinions about speckle. One opinion insists that speckle is solely noise to an ultrasound image and should be removed, since speckle significantly degrades the image quality, hence making it more difficult for the observer to discriminate the fine detail of images [130, 131]. This opinion is commonly accepted. The other opinion argues that speckle patterns reflect the local echogenicity of the underlying scatters which means speckle has underlying useful characters rather than merely being noise [135]. However, very little work has been done to explore the underlying characters of speckle. In this work, we treat speckle as noise and try to suppress speckle without destroying important features of the lesions. Two effective de-speckle methods are taken into consideration. One is the speckle reducing anisotropic diffusion (SRAD) [127], and the other is a newly published de-speckle method [132]. Both of the methods are good at removing the speckle noise and preserving the edges and details of the images at the same time. SRAD is a diffusion method in which the diffusion is edge-sensitive for speckled images. Its advantage is high speed and a good de-speckle effect. Anisotropic diffusion is frequently used in filtering techniques for speckle reduction. However, edge estimation using a gradient operator makes it difficult to handle a multiplicative noisy image. In order to eliminate such a disadvantage, SRAD is proposed particularly for envelope US images without logarithmic compression. In SRAD, the instantaneous coefficient of variation serves as the edge detector. The function exhibits high values at edges and produces low values in homogeneous regions. Thus, it ensures the mean-preserving behavior in the homogeneous regions, and edge-preserving and edge-enhancing at the edges. The method in [132] is a speckle reduction method tailored

especially for BUS images. It uses the local homogeneity defined by texture information to describe speckle noise. A 2-D homogeneity histogram is built, and the threshold is obtained using the maximal entropy principle. The pixels are divided into a homogenous set and a non-homogenous set based on the homogeneity threshold. The pixels in the non-homogeneous set are handled by the proposed directional average filters (DAF) iteratively. Figure 3.1 shows the results of the two methods. Obviously, the edges are better enhanced, and speckle noise is more effectively reduced by the method in [132] than the SRAD in [127]. Here a quantitative evaluation metric, the signal-to-mean square error (*SMSE*), is employed to evaluate the de-speckle effect [133]:

$$\text{SMSE} = 10\log_{10}\left(\frac{\sum_{i=1}^{k} S_i^2}{\sum_{i=1}^{k}(\hat{S}_i - S_i)^2}\right)$$

Where S_i is the *i*th pixel in the original image (speckle-free image), $\hat{S}_i$ is the *i*th pixel in the image after speckle reduction and *K* is the image size. A larger *SMSE* ratio means a better noise suppression effect. Since there is no speckle-free ultrasound image in reality; we use the method in [134] to approximate the speckle-free images by a homomorphic Wiener filter.

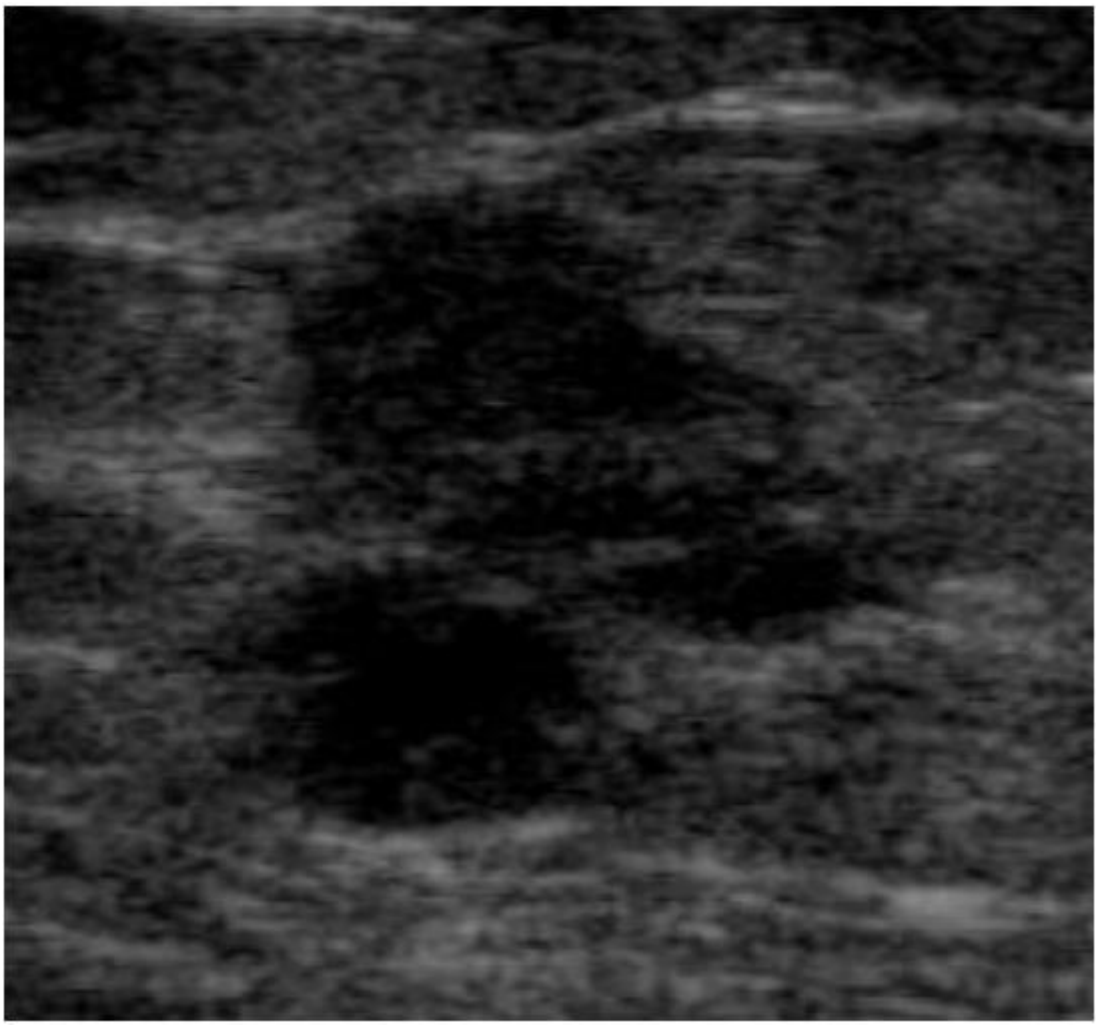

(a)

Figure 2.1: (a) The ROI cut from the original image.

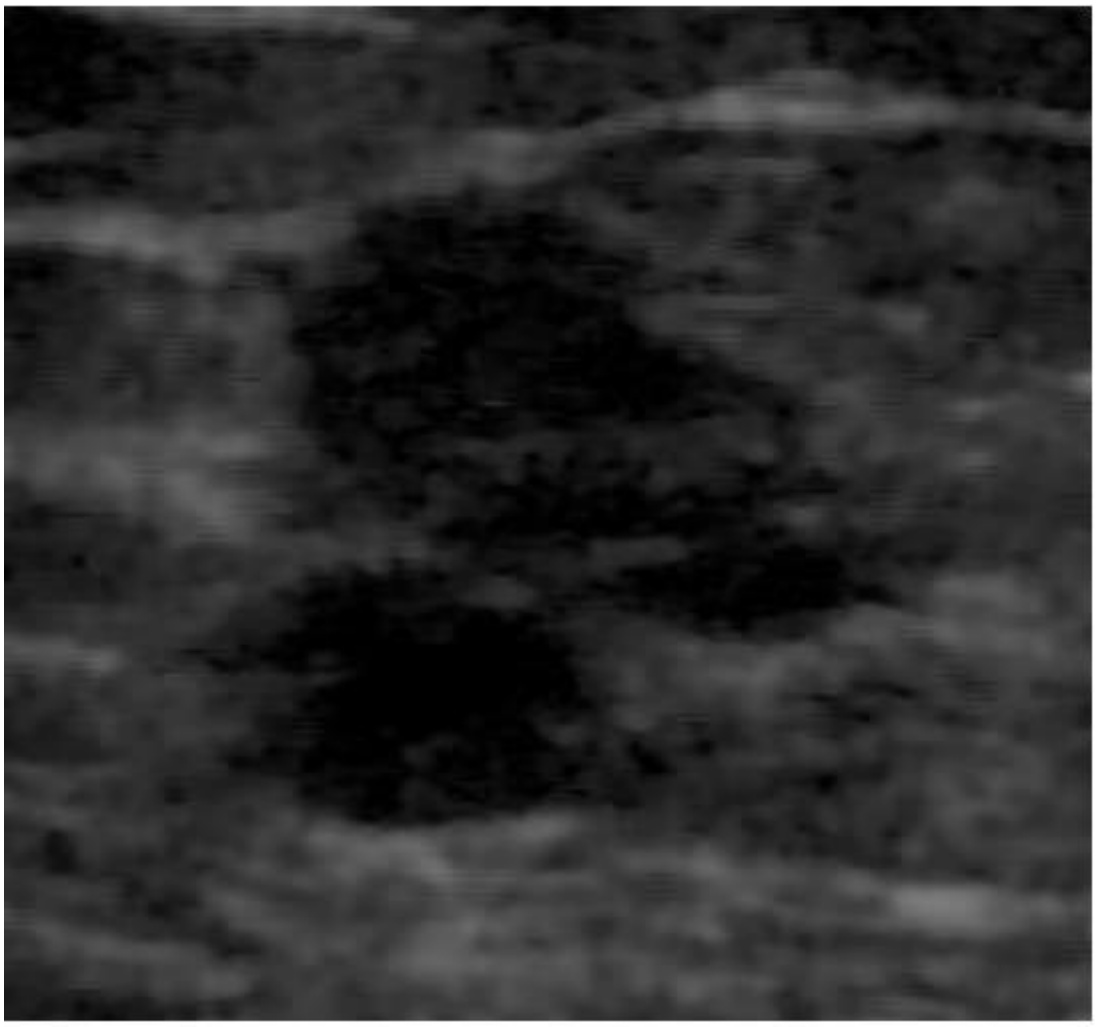

(b)

Figure 2.2: (b) Result of SRAD [127] after 5 iterations.

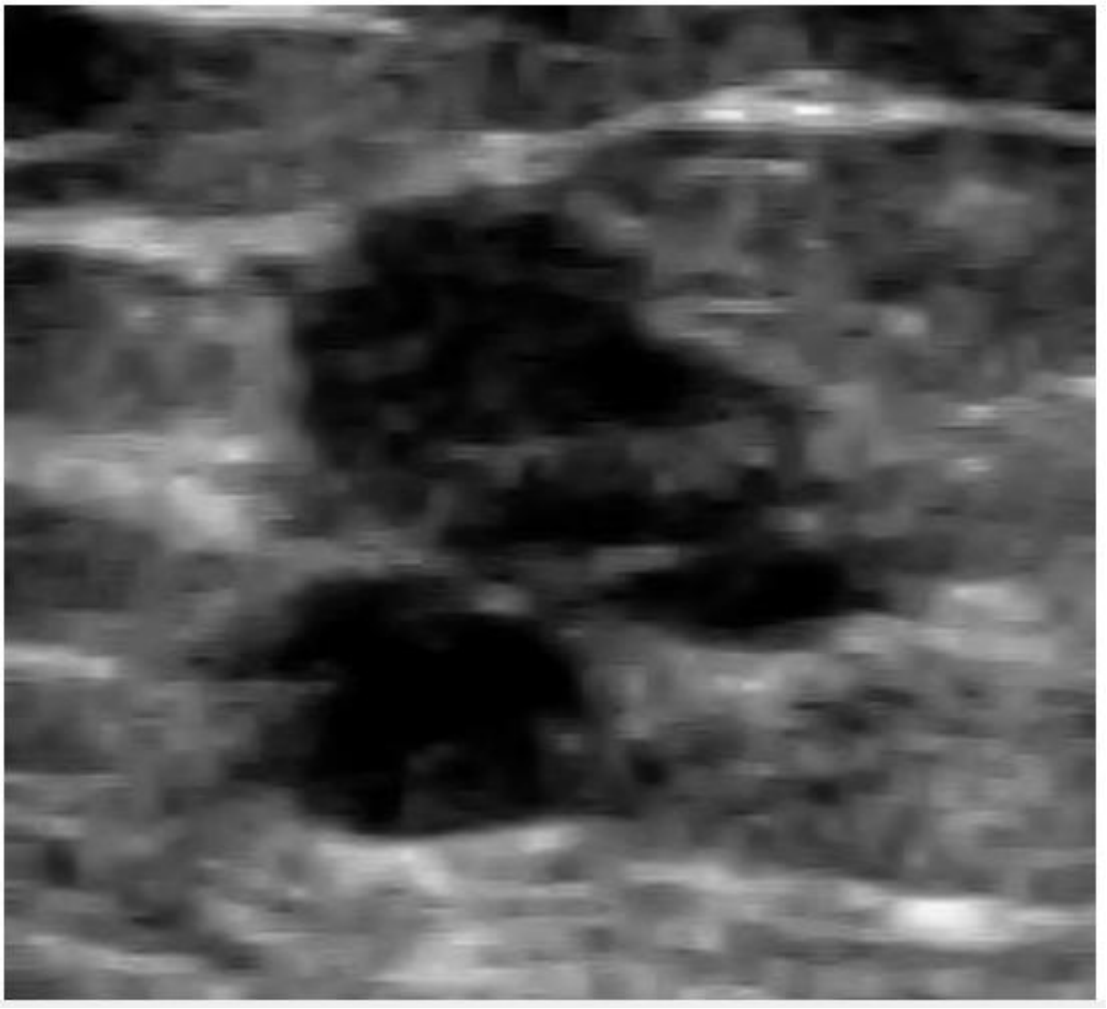

(c)

Figure 2.3: (c) Result of the method in [132]

A comparison between the two methods is conducted on the whole database. Both the de-speckle effect and time complexities are analyzed. As Table 3.1 shows, the average *SMSE* ratio of the method in [132] is higher than that of the SRAD method (30.80 over 16.66), while the average processing time of the method in [132] is longer than that of SRAD. Considering that the processing time (about 8 seconds) is acceptable for clinical application and the de-speckle effect is much better, we choose the method in [132] as the speckle reduction algorithm here.

Table 2.1 Comparison of De-speckle Effect and Time Complexity of the Method Described in [132] and SRAD in [127].

Methods	SMSE	Average processing time/case
De-speckle method in [58]	30.80	8.46 seconds
SRAD method in [50]	16.66	0.62 second

Chapter 3

IMPLIED SEGMENTATION METHODS & RESULT

The structures of BUS images vary a lot. It is very hard to find the lesion area from the BUS images. Selecting ROI is really helpful for better segmentation result. There are mainly two types of ROI. One type of ROI contains only the rough contour of the lesion and the other type of ROI contains both the contour of the lesion and background information. For selection of ROI it is not needed to find out the region boundary accurately because we just need to find a seed point inside the region boundary. We select the seed point based on the contrast amount.

3.1 Introduction

The early detection and diagnosis of cancer usually increases the chances of successful treatment. In addition, treatments for early cancer are often less complex and less expensive than treatments for more-advanced disease, sparing patients and their families greater hardship. However, too many cancers are still diagnosed at late stages, when effective treatment and long-term survival may not be possible.

Another promise of early detection is the identification of precancerous tissue abnormalities that are destined to become life-threatening cancers, providing an opportunity for even earlier intervention to prevent cancer from developing altogether. Similarly, the ability to accurately identify precancerous tissue abnormalities and early cancers that will not progress to potentially fatal malignancies would also be beneficial, potentially sparing many patients and their families the physical and financial harms of unnecessary treatment.

As has been true for many years, NCI continues to support a broad portfolio of research aimed at improving the early detection and diagnosis of cancer and its precursors. Two major goals of this research are increasing the dissemination of proven methods of detection and diagnosis and developing new and improved methods that are more accurate and of greater value clinically than those available today. Another goal is to produce technologies and tests

that are efficient and cost-effective and that can be used in all resource settings. Ultimately, this work should increase the number of cancers for which we have effective screening tests. The chances of successful early cancer detection and treatment depend on the clinical characteristics of the tumor and the screening strategy. If screening for early detection is to result in improved health in terms of reduced mortality, morbidity, and improved quality of life, specific conditions in both these areas must be fulfilled. If they are not, it is unlikely that screening can improve the health of the population in question. These conditions are as follow:

The incidence of a specific tumor in a target population must be sufficiently high to enable the available screening strategy to identify a significant number of tumors within a target population. Even if an annual screening test performs perfectly (i.e. all patients with cancer have a positive test result and all patients without cancer have a negative test result) but only one person in 10,000 will develop the cancer in any one year, then 10,000 people will have to be screened for every case that is to be diagnosed. The tumor must significantly reduce the quality or quantity of life of the patient. An example of a tumor that would not meet this criterion is basal cell carcinoma of the skin; it is slow growing and can easily be removed by minor surgery with minimal risk. The natural history of the tumor must include a sufficiently long asymptomatic period in which localized stages can be diagnosed and treated. The longer that the tumor remains localized during this asymptomatic period, the more likely the chance of diagnosing it at a curable stage. Cervical cancer is an example of a tumor that remains localized for up to 20 years or more during a long asymptomatic period . Uterine cancer, by comparison, while it may also remain localized for many years, often presents with vaginal bleeding in post menopausal women. Hence, over three quarters of the tumors are diagnosed at a localized stage because symptoms develop early (30). Cancer screening might therefore be expected to have greater impact on cervical cancer than on uterine cancer, as the former remains both localized and asymptomatic for an extended period of time.

There must be an effective treatment for tumors diagnosed at an early stage. For a treatment to be effective, it must (a) produce a better outcome in asymptomatic screened patients than in those who become symptomatic and seek medical care and (b) be widely available and acceptable to patients. The biologic characteristics of the tumor can create two biases that can lead investigators erroneously to conclude that screening has reduced the number

of deaths. Lead-time bias occurs when the early tumors diagnosed by screen-ing are not actually cured by treatment and patients ultimately die from the tumor anyway. Duration of survival, measured from time of diagnosis to time of death, will appear to have increased, but the actual time of death is unchanged. Length bias occurs because slower-growing tumors, which are likely to remain asymptomatic longer, are more likely to be found by screen-ing than fast growing tumors. The addition of the slower-growing tumors to the sample of tumors under observation produces a lower mortality rate in the screened population, even without treatment.

3.2 Implied Steps & Results

There are several steps we followed.

Step 1

A seed point is the starting point for region growing. Its selection is important to the segmentation result. If a seed point is selected outside the region of interest (ROI), the final segmentation result would definitely be incorrect. Due to the low quality of US images, most region growing methods require the seed point be selected manually in advance. In order to make the region growing fully automatic, it is necessary to develop an automatic seed point selection method for BUS images. However, very little research has been done in this area; thus, relevant work is rare and immature. Poonguzhali and Ravindran [51] proposed an automatic method to select seed point for masses using both the co-occurrence and run length features. The run length features were calculated around the points selected by the co-occurrence features. If all the run length features of a selected point and its neighborhood points were equal, the point was considered as a seed point. In [21], after several preprocessing steps, a seed point score formula was used to evaluate a set of randomly selected points. The point with the highest score was considered as the seed point. In yet another method [52], after preprocessing and morphological operations, a binary image was obtained and the sum of the pixels on each row and column are computed. Indexes of the seed point were found as the row and column number with the max sums, respectively. All the aforementioned methods took into account only the statistics of the texture features for a mass region (i.e., the mass is darker than the surrounding tissues and more homogeneous than other regions). They failed to consider spatial features of a US mass (such as the fact that

a mass frequently appears at the upper part of image and is barely connected with the image boundary).

Step 2:

For edge detection we choose the canny edge detection algorithm. Canny edge detection is a technique to extract useful structural information from different vision objects and dramatically reduce the amount of data to be processed. It has been widely applied in various computer vision systems. Canny has found that the requirements for the application of edge detection on diverse vision systems are relatively similar. Thus, an edge detection solution to address these requirements can be implemented in a wide range of situations. The general criteria for edge detection include:

Detection of edge with low error rate, which means that the detection should accurately catch as many edges shown in the image as possible

The edge point detected from the operator should accurately localize on the center of the edge.

A given edge in the image should only be marked once, and where possible, image noise should not create false edges.

The Process of Canny edge detection algorithm can be broken down to 5 different steps:

Apply Gaussian filter to smooth the image in order to remove the noise

Find the intensity gradients of the image

Apply non-maximum suppression to get rid of spurious response to edge detection

Apply double threshold to determine potential edges

Track edge by hysteresis: Finalize the detection of edges by suppressing all the other edges that are weak and not connected to strong edges.

Since all edge detection results are easily affected by image noise, it is essential to filter out the noise to prevent false detection caused by noise. To smooth the image, a Gaussian filter is applied to convolve with the image. This step will slightly smooth the image to reduce the effects of obvious noise on the edge detector. The equation for a Gaussian filter kernel of size $(2k+1)\times(2k+1)$ is given by:

$$H_{ij} = \frac{1}{2\pi\sigma^2} \exp\left(-\frac{(i-(k+1))^2 + (j-(k+1))^2}{2\sigma^2} \right); 1 \leq i, j \leq (2k+1)$$

An edge in an image may point in a variety of directions, so the Canny algorithm uses four filters to detect horizontal, vertical and diagonal edges in the blurred image. The edge detection operator (such as Roberts, Prewitt, or Sobel) returns a value for the first derivative in the horizontal direction (G_x) and the vertical direction (G_y). From this the edge gradient and direction can be determined:

$$\mathbf{G} = \sqrt{\mathbf{G}_x{}^2 + \mathbf{G}_y{}^2}$$

$$\mathbf{\Theta} = \operatorname{atan2}(\mathbf{G}_y, \mathbf{G}_x),$$

where G can be computed using the hypo function and atan2 is the arctangent function with two arguments. The edge direction angle is rounded to one of four angles representing vertical, horizontal and the two diagonals (0°, 45°, 90° and 135°). An edge direction falling in each color region will be set to a specific angle values, for instance θ in [0°, 22.5°] or [157.5°, 180°] maps to 0°.

Non-maximum suppression is an edge thinning technique. Non-maximum suppression is applied to find "the largest" edge. After applying gradient calculation, the edge extracted from the gradient value is still quite blurred. With respect to criterion 3, there should only be one accurate response to the edge. Thus non-maximum suppression can help to suppress all the gradient values (by setting them to 0) except the local maxima, which indicate locations with the sharpest change of intensity value. The algorithm for each pixel in the gradient image is:

Compare the edge strength of the current pixel with the edge strength of the pixel in the positive and negative gradient directions.

If the edge strength of the current pixel is the largest compared to the other pixels in the mask with the same direction (i.e., the pixel that is pointing in the y-direction, it will be compared to the pixel above and below it in the vertical axis), the value will be preserved. Otherwise, the value will be suppressed.

After application of non-maximum suppression, remaining edge pixels provide a more accurate representation of real edges in an image. However, some edge pixels remain that are caused by noise and color variation. In order to account for these spurious responses, it is essential to filter out edge pixels with a weak gradient value and preserve edge pixels with a high gradient value. This is accomplished by selecting high and low threshold values. If an edge pixel's gradient value is higher than the high threshold value, it is marked as a strong edge pixel. If an edge pixel's gradient value is smaller than the high threshold value and larger than the low threshold value, it is marked as a weak edge pixel. If an edge pixel's value is smaller than the low threshold value, it will be suppressed. The two threshold values are empirically determined and their definition will depend on the content of a given input image. To track the edge connection, blob analysis is applied by looking at a weak edge pixel and its 8-connected neighborhood pixels. As long as there is one strong edge pixel that is involved in the blob, that weak edge point can be identified as one that should be preserved.

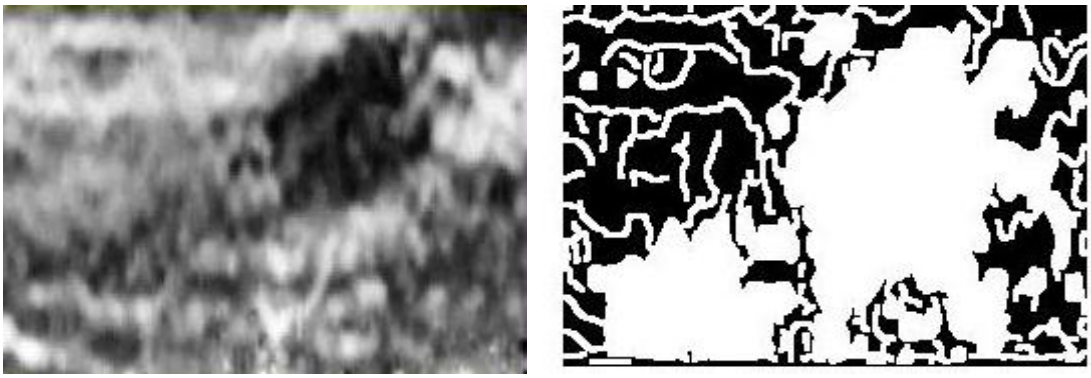

Figure 2.1: Before applying canny filter (left) and after applying canny filter (right)

Step 3:

Canny filter converts images into binary images. Thus, we can detect the quality of images counting both black and white pixels of images. Statistically, filtered images of malignant cells contain higher number of white pixels. Hence, we rank these images in groups based on their total number of white pixels. Each group contains 10 images. We extracted images from video and serially numbered them. As a result, we get almost same type of 2-3 images before and after an image. So, we count total number of white pixels in each of these closely matched images. Afterwards, we rank them from higher to lower number of white pixels. The we apply Adaptive Histogram Equalization on these images to enhance the contrast of the grayscale

images by transforming the values using contrast-limited adaptive histogram equalization (CLAHE). CLAHE operates on small regions in the image, called tiles, rather than the entire image. Each tile's contrast is enhanced, so that the histogram of the output region approximately matches the histogram specified by the 'Distribution' parameter. The neighboring tiles are then combined using bilinear interpolation to eliminate artificially induced boundaries. The contrast, especially in homogeneous areas, can be limited to avoid amplifying any noise that might be present in the image.

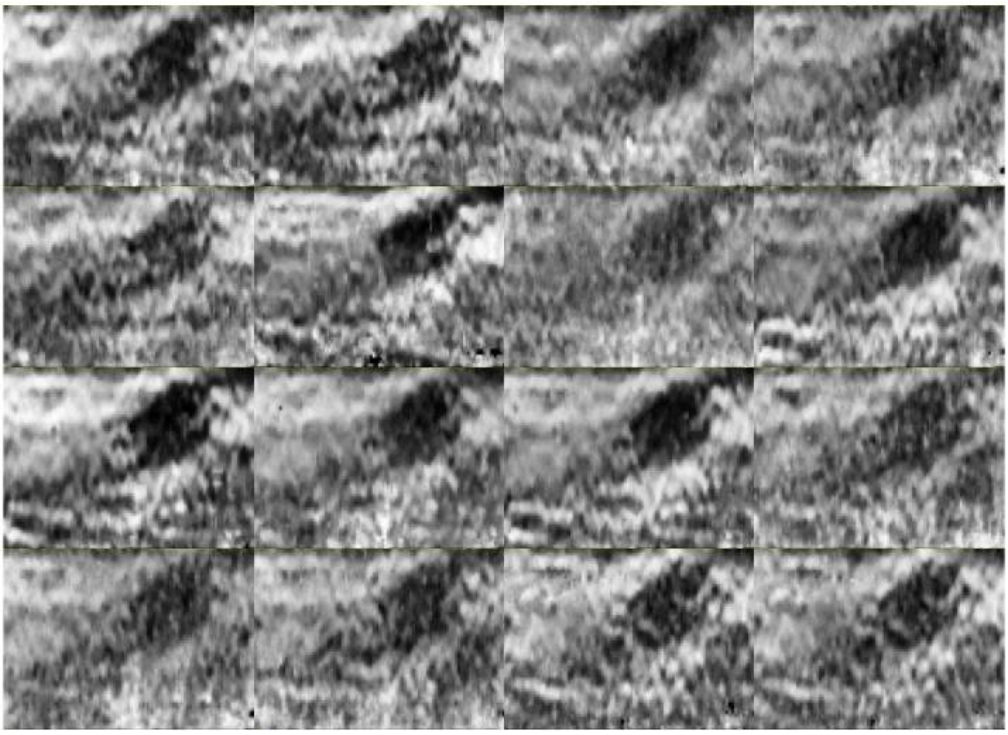

Figure 2.2: Before applying adaptive histogram equalization on the best frames.

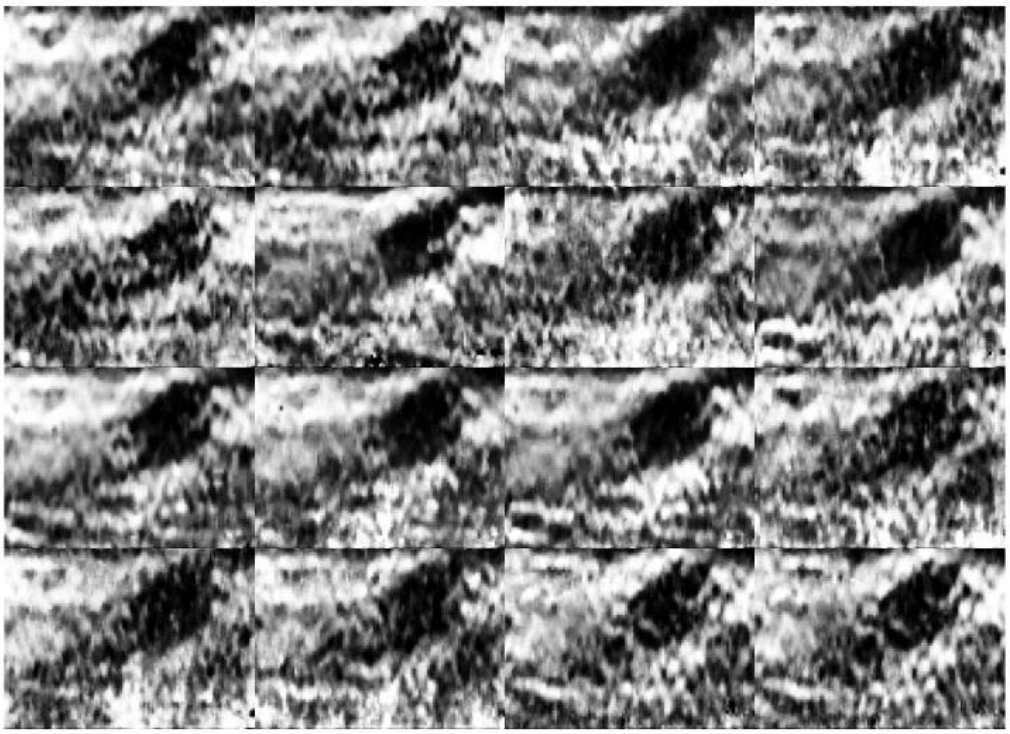

Figure 2.3: After applying adaptive histogram equalization on the best frames.

Step 4:

For finding out a group of best images we correlate all these filtered images with the best one we got from these set of images. Commonly, Digital image correlation relies on finding the maximum of the correlation array between pixel intensity array subsets on two or more corresponding images, which gives the integer translational shift between them. It is also possible to estimate shifts to a finer resolution than the resolution of the original images, which is often called "subpixel" registration because the measured shift is smaller than an integer pixel unit. For subpixel interpolation of the shift, there are other methods that do not simply maximize the correlation coefficient. An iterative approach can also be used to maximize the interpolated correlation coefficient by using nonlinear optimization techniques. The nonlinear optimization approach tends to be conceptually simpler, but as with most nonlinear optimization techniques, it is quite slow, and the problem can sometimes be reduced to a much faster and more stable linear optimization in phase space.

The two-dimensional discrete cross correlation r_{ij} can be defined several ways, one possibility being:

Cross correlation is implemented as

$$r_{ij} = \frac{\sum_m \sum_n [f(m+i, n+j) - \bar{f}][g(m,n) - \bar{g}]}{\sqrt{\sum_m \sum_n [f(m,n) - \bar{f}]^2 \sum_m \sum_n [g(m,n) - \bar{g}]^2}}.$$

Here f(m, n) is the pixel intensity or the gray-scale value at a point (m, n) in the original image, g(m, n) is the gray-scale value at a point (m, n) in the translated image, $\bar{f}$ and $\bar{g}$ are mean values of the intensity matrices f and g respectively.

However, in practical applications, the correlation array is usually computed using Fourier-transform methods, since the fast Fourier transform is a much faster method than directly computing the correlation.

$$\mathbf{F} = \mathcal{F}\{f\}, \quad \mathbf{G} = \mathcal{F}\{g\}.$$

Then taking the complex conjugate of the second result and multiplying the Fourier transforms together elementwise, we obtain the Fourier transform of the correlogram, R:

$$R = \mathbf{F} \circ \mathbf{G}^*,$$

where $\circ$ is the Hadamard product (entry-wise product). It is also fairly common to normalize the magnitudes to unity at this point, which results in a variation called phase correlation. Then the cross-correlation is obtained by applying the inverse Fourier transform:

$$r = \mathcal{F}^{-1}\{R\}.$$

At this point, the coordinates of the maximum of r_{ij} give the integer shift:

$$(\Delta x, \Delta y) = \arg\max_{(i,j)}\{r\}.$$

Step 5:

We implemented watershed transformation in the images for higher accuracy. The term watershed refers to a ridge that divides areas drained by different river systems. The watershed transform finds "catchment basins" or "watershed ridge lines" in an image by

treating it as a surface where light pixels represent high elevations and dark pixels represent low elevations. The elements of L are integer values greater than or equal to 0. The elements labeled 0 do not belong to a unique watershed region. The elements labeled 1 belong to the first watershed region, the elements labeled 2 belong to the second watershed region, and so on. By default, watershed uses 8-connected neighborhoods for 2-D inputs and 26-connected neighborhoods for 3-D inputs. For higher dimensions, watershed uses the connectivity given by conndef(ndims(A),'maximal'). Then we convert the image returned after watershed into an RGB color image for the purpose of visualizing the labeled regions. The label2rgb function determines the color to assign to each object based on the number of objects in the label matrix. The label2rgb function picks colors from the entire range of the color map. Then we use strel to represent a flat morphological structuring element, which is an essential part of morphological dilation and erosion operations. A flat structuring element is a binary valued neighborhood, either 2-D or multidimensional, in which the true pixels are included in the morphological computation, and the false pixels are not. The center pixel of the structuring element, called the origin, identifies the pixel in the image being processed. Use the strel function (described below) to create a flat structuring element. You can use flat structuring elements with both binary and grayscale images. The following figure illustrates a flat structuring element.

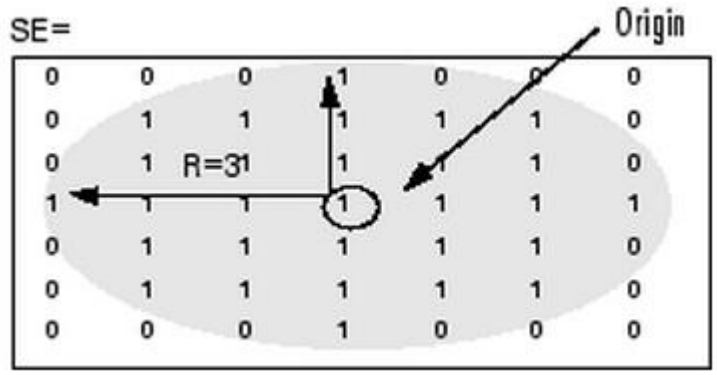

After that we erode the image and perform morphological reconstruction of the image marker under the image mask. marker and mask can be two intensity images or two binary images with the same size. The returned image IM is an intensity image or a binary image, depending on the input images, and is the same size as the input images.

marker must be the same size as mask, and its elements must be less than or equal to the corresponding elements of mask. If the values in marker are greater than corresponding

elements in mask, imreconstruct clips the values to the mask level before starting the procedure. Then we dilate the grayscale, binary, or packed binary image and complement the binary image. Zeros become ones and ones become zeros; black and white are reversed. In the complement of an intensity or RGB image, each pixel value is subtracted from the maximum pixel value supported by the class (or 1.0 for double-precision images) and the difference is used as the pixel value in the output image. In the output image, dark areas become lighter and light areas become darker. Then we trace the boundaries of the images in the best frames which we obtained earlier.

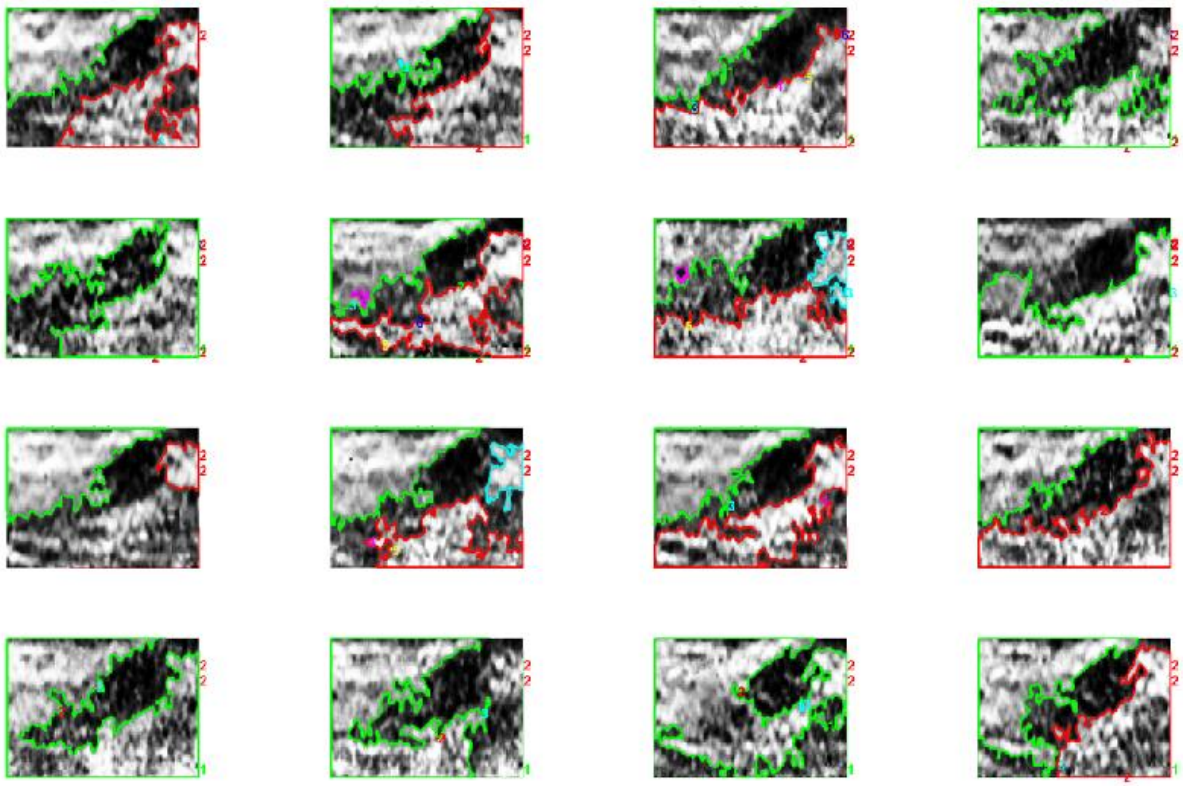

Figure 2.4: 16 best frame indicating the exact location and size of tumor.

Chapter 4

CONCLUSION & FUTURE WORK

In this dissertation, we study lesion boundary detection for breast ultrasound images and propose a novel lesion segmentation method. The proposed segmentation method is composed of several steps: automatic ROI generation, speckle reduction, contrast enhancement, and neutrosophic l -means clustering (NLM). Automatic ROI (region of interest) generation facilitates the full automation of the segmentation method and speeds up the segmentation process. Complicated background is removed from the image; hence, the method focuses on the lesion area rather than the entire image, and segmentation accuracy is improved. Two different speckle reduction methods are studied, and one is used in this work as a preprocessing step. A novel local phase feature PMO is proposed and utilized to enhance the contrast and quality for the BUS images. In the neutrosophic l -means clustering, the neutrosophy, a new branch of philosophy, is applied to image segmentation. Through a comparison with traditional fuzzy c-means, the positive effect of applying neutrosophy is demonstrated. To evaluate the whole segmentation method proposed in this work, a quantitative analysis of both accuracy and efficiency are conducted on the database composed of 60 BUS images. Comparison with other BUS image segmentation methods using the same database proves the superiority of the proposed method. Finally, sensitivity analysis shows the robustness of the newly proposed segmentation method.

The advantages of the proposed method can be summarized as:

It is completely automatic.

It finds the accurate lesion boundaries even in complicated and low-contrast BUS images.

In accuracy, it outperforms the fuzzy c-means clustering as well as three other BUS segmentation methods. Experiments are carried out using a common database and the performance is evaluated by a set of comprehensive criteria.

The analysis time of the proposed method is about 20 seconds for each case, which is more efficient than the active-contour-based method and the level-set-based method. The watershed-based-method is the fastest, but unfortunately it trades speed for accuracy, with its accuracy rate being the lowest among the methods studied in this work.

The proposed method is quite robust.

One limitation of the proposed method is that it sometimes fails in cases containing large posterior shadowing areas connected with the lesion. A second limitation of the proposed method is that it can detect the contours of only one lesion per image. These problems will be addressed in future research. Another future direction is to use this method for other applications, such as echocardiography, prostate ultrasound, etc. Since this method is based on the characteristics of ultrasound imaging, it should be easily adjusted for other ultrasound images. Future work also includes classifying the lesions into benign/malignant based on the features extracted from the segmentation results.

REFERENCES

1. https://www.wcrf.org/dietandcancer/cancer-trends/breast-cancer-statistics

2. https://www.bcrf.org/breast-cancer-statistics

3. Vineeta Singh, Christobel Saunders, Liz Wylie & Anita Bourk : New diagnostic techniques for breast cancer detection. 1-3

4. Juan Shan: A FULLY AUTOMATIC SEGMENTATION METHOD FOR BREAST ULTRASOUND IMAGES. 1,2

5. Fischer U, Baum F, Obenauer S,Luftner-Nagel S, Von Heyden D, Vosshenrich R: Comparative study in patients with microcalcifications: full-field digital mammography vs screen-film mammography. Eur. Radiol. 12, 2679–2683 (2002)

6. Berry DA: Benefits and risks of screening mammography for women in their forties: a statistical appraisal. J. Natl Cancer Inst. 90, 1431–1439 (1998)

7. Nystrom L, Andersson I, Bjurstam N, Frisell J, Nordenskjold B, Rutqvist LE: Long-term effects of mammography screening: updated overview of the Swedish randomised trials. Lancet 359, 909–919 (2002)

8. Mandelson MT, Oestreicher N, Porter PL et al.: Breast density as a predictor of mammographic detection: comparison of interval- and screen-detected cancers. J. Natl Cancer Inst. 92, 1081–1087 (2000)

9. Carney PA, Miglioretti DL, Yankaskas BC et al.: Individual and combined effects of age, breast density, and hormone replacement therapy use on the accuracy of screening mammography. Ann. Intern. Med. 138, 168–175 (2003).

10. Brown ML, Houn F, Sickles EA, Kessler LG: Screening mammography in community practice: positive predictive value of abnormal findings and yield of follow-up diagnostic procedures. AJR Am. J. Roentgenol. 165, 1373–1377 (1995).

11. Barton MB, Moore SM, Polk S, Shtatland E, Elmore JG, Fletcher SW: Increased patient concern after false-positive mammograms: clinician documentation and subsequent ambulatory visits. J. Gen. Intern. Med. 16, 150–156 (2001).

12. Christiansen CL, Wang F, Barton MB et al.: Predicting the cumulative risk of false - positive mammograms. J. Natl Cancer Inst. 92, 1657–1666 (2000)

13. Ma L, Fishell EK, Wright B, Hanna W, Allan S, Boyd NF: Case–control study of factors associated with failure to detect breast cancer by mammography. J. Natl Cancer Inst. 84, 781–785 (1992)

14. Freer TW, Ulissey MJ: Screening mammography with computer-aided detection: prospective study of 12,860 patients in a community breast center Radiology 220, 781–786 (2001)

15. Gur D, Sumkin JH, Rockette HE et al.: Changes in breast cancer detection and mammography recall rates after the introduction of a computer-aided detection system. J. Natl Cancer Inst. 96, 185–190 (2004).

16. Vyborny CJ: Can computers help radiologists read mammograms? Radiology 191, 315-317 (1994)

17. Warren Burhenne LJ, Wood SA, D'Orsi CJ et al.: The potential contribution of computer-aided detection to the sensitivity of screening mammography. Radiology 215, 554 –562 (2000).

18. Hendee WR, Beam C, Hendrick E: Proposition: all mammograms should be double-read. Med. Phys. 26, 115–118 (1999).

19. Freer TW, Ulissey MJ: Screening mammography with computer-aided detection: prospective study of 12,860 patients in a community breast center. Radiology 220, 781–786 (2001).

20. Jiang Y, Nishikawa RM, Schmidt RA et al.: Improving breast cancer diagnosis with computer-aided diagnosis. Acad. Radiol. 6, 22–33 (1999).

21. Fenton JJ, Taplin SH, Carney PA et al.: Influence of computer-aided detection on performance of screening mammogram. N. Engl. J. Med. 356(14), 1399–1409 (2007).

22. Planche K, Vinnicombe S: Breast imaging in the new era. Cancer Imaging 4(2), 39–50 (2004).

23. https://www.radiologyinfo.org/en/info.cfm?pg=tomosynthesis

24. Niklason LT, Christian BT, Niklason LE, et al. Digital tomosynthesis in breast imaging. Radiology 1997;205(2):399–406.

25. Sechopoulos I. A review of breast tomosynthesis. Part I. The image acquisition process. Med Phys 2013;40(1):014301.

26. Sechopoulos I. A review of breast tomosynthesis. Part II. Image reconstruction, processing and analysis, and advanced applications. Med Phys 2013;40(1): 014302.

27. Gordon PB: Ultrasound for breast cancer screening and staging. Radiol. Clin. N. Am. 40, 431–441 (2002)

28. Diekmann F, Diekmann S, Richter K et al.: Near monochromatic x-rays for digital

slot-scan mammography: initial findings. Eur. Radiol. 14(9), 1641–1646 (2004).

29. Crystal P, Strano SD, Shcharynski S et al.: Using sonography to screen women with mammographically dense breasts. AJR Am.J. Roentgenol. 181, 177–182 (2003)

30. Harvey JA: Sonography of palpable breast masses. Semin. Ultrasound CT MR 27(4), 284–297 (2006).

31. Berg WA: Beyond standard mammographic screening: mammography at age extremes, ultrasound, and MR imaging. Radiol. Clin. North Am. 45(5), 895–906 (2007).

32. Yang WT, Ahuja A, Tang A et al.: High resolution sonographic detection of axillary lymph node metastases in breast cancer. J. Ultrasound Med. 15(3), 241–246 (1996).

33. Berg WA, Blume JD, Cormack JB, Mendelson EB, Madsen EL; ACRIN 6666 Investigators: Lesion detection and characterization in a breast US phantom:
results of the ACRIN 6666. Radiology 239(3), 693–702 (2006).

34.
https://www.physics.utoronto.ca/~jharlow/teaching/phy138_0708/lec04/ultrasoundx.htm

35. Hwang, K.-H., H., Lee, J.G., Kim, J.H., Lee, H.-J. Om, K.-S., Yoon, M., and Choe, W. Computer aided diagnosis (CAD) of breast mass on ultrasonography and scintimammography. In Proceedings of 7th International Workshop on Enterprise Networking and Computing in Healthcare Industry, 2005, 187-189

36. American-College-of-Radiology, ACR standards 2000-2001. 2000: Reston, VA.

37. Noble, J.A. and Boukerroui, D. Ultrasound image segmentation: A survey. IEEE Trans. on Medical Imaging 25, 8 (2006), 987-1010.

38. Joo, S., Moon, W.K., and Kim, H.C. Computer-aided diagnosis of solid breast nodules on ultrasound with digital image processing and artificial neural network. In 26th Annual IEEE International Conference Proceedings on Engineering in Medicine and Biology Society, 2004, 1397-13400.

39. Chen, D.-R., Chang, R.-F., and Huang, Y.-L. Computer-aided diagnosis applied to US of solid breast nodules by using neural networks. Radiology 213, 2 (1999), 407-412.

40. Madabhushi, A. and Metaxas, D.N. Combining low-, high-level and empirical domain knowledge for automated segmentation of ultrasonic breast lesions. IEEE Trans. on Medical Imaging 22, 2 (2003), 155-169.

41. Xiaohui, H., Bruce, C.J., Pislaru, C., and Greenleaf, J.F. Segmenting highfrequency intracardiac ultrasound images of myocardium into infarcted, ischemic, and normal regions. IEEE Trans. on Medical Imaging 20, 12 (2001), 1373-1383.

42. Joo, S., Yang, Y.S., Moon, W.K., and Kim, H.C. Computer-aided diagnosis of solid breast nodules: Use of an artificial neural network based on multiple sonographic features. IEEE Trans. on Medical Imaging 23, 10 (2004), 1292-1300.

43. Yeh, C.-K., Chen, Y.-S., Fan, W.-C., and Liao, Y.-Y. A disk expansion segmentation method for ultrasonic breast lesions. Pattern Recognition 42, 5(2009), 596-606

44. Drukker, K., Giger, M.L., Horsch, K., Kupinski, M.A., Vyborny, C.J., and Mendelson, E.B. Computerized lesion detection on breast ultrasound. Medical Physics 29, 7 (2002), 1438-1446.

45. Horsch, K., Giger, M.L., Venta, L.A., and Vyborny, C.J. Computerized diagnosis of breast lesions on ultrasound. Medical Physics 29, 2 (2002), 157-164.

46. Horsch, K., Giger, M.L., Venta, L.A., and Vyborny, C.J. Automatic segmentation of breast lesions on ultrasound. Medical Physics 28, 8 (2001), 1652-1659.

47. Liu, B., Cheng, H.D., Huang, J., Tian, J., Liu, J., and Tang, X., Automated segmentation of ultrasonic breast lesions using statistical texture classification and active contour based on probability distance. Ultrasound in Medicine & Biology 35, 8 (2009), 1309-1324.

48. Sarti, A., Corsi, C., Mazzini, E., and Lamberti, C. Maximum likelihood segmentation with Rayleigh distribution of ultrasound images. Computers in Cardiology 31 (2004), 329-332.

49. Chang, R.-F., Wu, W.-J., Moon, W.K., Chen, W.-M., Lee, W., and Chen, D.-R. Segmentation of breast tumor in three-dimensional ultrasound images using threedimensional discrete active contour model. Ultrasound in Medicine & Biology 29, 11 (2003), 1571-1581.

50. Chen, D.-R., Chang, R.-F., Wu, W.-J., Moon, W.K., and Wu, W.-L. 3-D breast ultrasound segmentation using active contour model. Ultrasound in Medicine & Biology 29, 7 (2003), 1017-1026.

51. Chang, R.F., Wu, W.J., Tseng, C., Chen, D.R., and Moon, W.K. 3-D snake for US in margin evaluation for malignant breast tumor excision using mammotome. IEEE Trans. on Information Technology in Biomedicine 7, 3 (2003), 197-201.

52. Sahiner, B., Chan, H.-P., Roubidoux, M.A., Helvie, M.A., Hadjiiski, L.M., Ramachandran, A., Paramagul, C., LeCarpentier, G.L., Nees, A., and Blane, C. Computerized characterization of breast masses on three-dimensional ultrasound volumes. Medical Physics 31, 4 (2004), 744-754.

53. Boukerroui, D., Baskurt, A., Noble, J.A., and Basset, O. Segmentation of ultrasound images--multiresolution 2D and 3D algorithm based on global and local statistics. Pattern Recognition Letters 24, 4-5 (2003), 779-790.

54. Xiao, G., Brady, M., Noble, J.A., and Zhang, Y. Segmentation of ultrasound Bmode images with intensity inhomogeneity correction. IEEE Trans. on Medical Imaging 21, 1 (2002), 48-57.

55. Cheng, H.D., Hu, L.M., Tian, J.W., and Sun, L., A novel Markov random field segmentation algorithm and its application to breast ultrasound image analysis. In 6th International Conference on Computer Vision, Pattern Recognition and Image Processing, 2005, 644-647.

56. Boukerroui, D., Basset, O., Guérin, N., and Baskurt, A. Multiresolution texture based adaptive clustering algorithm for breast lesion segmentation. European J. Ultrasound 8, 2 (1998), 135-144.

57. Christopher, L.A., Delp, E.J., Meyer, C.R., and Carson, P.L. 3-D Bayesian ultrasound breast image segmentation using the EM/MPM algorithm. In Proceedings of IEEE International Symposium on Biomedical Imaging, 2002, 86-89.

58. Kotropoulos, C. and Pitas, I. Segmentation of ultrasonic images using support vector machines. Pattern Recogniton Letters 24, 4-5 (2003), 715-727.

59. Zhan, Y. and Shen, D. Deformable segmentation of 3-D ultrasound prostate images using statistical texture matching method. IEEE Trans. on Medical Imaging 25, 3 (2006), 256-272.

60. Wu, H.-M. and Lu, H.H.-S. Iterative sliced inverse regression for segmentation of ultrasound and MR images. Pattern Recognition 40, 12 (2007), 3492-3502.

61. Dokur, Z. and Ölmez, T. Segmentation of ultrasound images by using a hybrid neural network. Pattern Recognition Letters 23, 14 (2002), 1825-1836.

62. Iscan, Z., Kurnaz, M.N., Dokur, Z., and Ölmez, T. Letter: Ultrasound image segmentation by using wavelet transform and self-organizing neural network. Neural Information Processing - Letters and Reviews 10, 8-9 (2006).

63. Huang, Y.-L. and Chen, D.-R. Watershed segmentation for breast tumor in 2-D sonography. Ultrasound in Medicine & Biology 30, 5 (2004), 625-632.

64. Gomez, W., Leija, L., Alvarenga, A.V., Infantosi, A.F.C., and Pereira, W.C.A. Computerized lesion segmentation of breast ultrasound based on markercontrolled watershed transformation. Medical Physics 37, 1 (2010), 82-95.

65. Huang, C.S., Wu, C.Y., Chu, J.S., Lin, J.H., Hsu, S.M., and Chang, K.J. Microcalcifications of non-palpable breast lesions detected by ultrasonography: correlation with mammography and histopathology. Ultrasound in Obstetrics and Gynecology 13, 6 (1999), 431-436.

66. Chen, C.-M., Chou, Y.-H., Chen, C.S.K., Cheng, J.-Z., Ou, Y.-F., Yeh, F.-C., and Chen, K.-W. Cell-competition algorithm: A new segmentation algorithm for multiple objects with irregular boundaries in ultrasound images. Ultrasound in Medicine & Biology 31, 12 (2005), 1647-1664.

67. Cheng, J.-Z., Chou, Y.-H., Huang, C.-S., Chang, Y.-C., Tiu, C.-M., Yeh, F.-C., Chen, K.-W., Tsou, C.-H., and Chen, C.-M. ACCOMP: Augmented cell competition algorithm for breast lesion demarcation in sonography. Medical Physics 37, 12 (2010), 6240-6252

68. Cheng, J.-Z., Chen, C.-M., Chou, Y.-H., Chen, C.S.K., Tiu, C.-M., and Chen, K.-W. Cell-based two-region competition algorithm with a map framework for boundary delineation of a series of 2D ultrasound smages. Ultrasound in Medicine & Biology 33, 10 (2007), 1640-1650

69. Feig SA, Yaffe MJ: Digital mammography, computer-aided diagnosis, and telemammography. Radiol. Clin. North Am. 33, 1205–1230 (1995).

70. Kegelmeyer WP, Pruneda JM, Bourland PD et al.: Computer-aided mammographic screening for spiculated lesions. Radiology 191, 331–337 (1994)

71. Pisano ED, Gatsonis C, Hendrick E et al.: Diagnostic performance of digital versus film mammography for breast-cancer screening. N. Engl. J. Med. 353, 1773–1783 (2005).

72. Fischmann A, Seigmann KC, Wersebe A, Clausenn CD: Comparison of full-field

digital mammography and film-screen mammography: image quality and lesion detection. Br. J. Radiol. 78, 312–315 (2005)

73. Lewin JM, D'Orsi CJ, Hendrick RE, Moss LJ, Isaacs PK, Karellas A: Clinical comparison of full-field digital mammography and screen-film mammography for detection of breast cancer. AJR Am. J. Roentgenol. 179, 671–677 (2002)

74. Kuhl CK, Mielcareck P, Klaschik S et al.: Dynamic breast MR imaging: are signal intensity time course data useful for differential diagnosis of enhancing lesions? Radiology 211(1), 101–110 (1999).

75. Kuhl CK, Schild HH, Morakkabati N: Dynamic bilateral contrast enhanced MR imaging of breast: trade off between spatial and temporal resolution. Radiology 236(3), 789–800 (2005).

76. Diekmann F, Diekmann S, Jeunehomme F, Muller S, Hamm B, Bick U: Digital mammography using iodine based contrast media: initial clinical experience with dynamic contrast medium enhancement. Invest. Radio. 40(7), 397–404 (2005).

77. Diekmann F, Bick U: Tomosynthesis and contrast-enhanced digital mammography: recent advances in digital mammography. Eur. Radiol. 17, 3086–3092 (2007).

78. Bluemke DA, Gatsonis CA, Chen MH et al.: MR imaging prior to breast biopsy: results of the International Breast Magnetic Resonance Consortium (IBMC) trial. JAMA 292, 2735–2742 (2004).

79. Heywang-Köbrunner SH, Viehweg P, Heinig A, Kuchler C: Contrast-enhanced MRI of the breast: accuracy, value, controversies, solutions. Eur. J. Radiol. 24, 94–108 (1997).

80. Gilles R, Guinebretiere JM, Shapeero LG et al.: Assessment of breast cancer recurrence

with contrast-enhanced subtraction MR imaging: preliminary results in 26 patients. Radiology 188(2), 473–478 (1993).

81. Warner E, Plewes DB, Hill KA et al.: Surveillance of BRCA1 and BRCA2 mutation carriers with magnetic resonance imaging, ultrasound, mammography, and clinical breast examination. JAMA 292, 1317–1325 (2004).

82. Saslow D, Boetes C, Burke W et al.: American Cancer Society guidelines for breast screening with MRI as an adjunct to mammography. CA Cancer J. Clin. 57, 75–89 (2007).

83. Olson JA Jr, Morris EA, van Zee KJ, Linehan DC, Borgen PI: Magnetic resonance imaging facilitates breast conservation for occult breast cancer. Ann. Surg. Oncol. 7, 411–415 (2000).

84. Herrada J, Iyer RB, Atkinson EN, Sneige N, Buzdar AU, Hortobagyi GN: Relative value of physical examination, mammography, and breast sonography in evaluating the size of the primary tumor and regional lymph node metastases in women receiving neoadjuvant chemotherapy for locally advanced breast carcinoma. Clin. Cancer Res. 3, 1565–1169 (1997).

85. Balu-Maestro C, Chapellier C, Bleuse A, Chanalet I, Chauvel C, Largillier R: Imaging in evaluation of response to neoadjuvant breast cancer treatment benefits of MRI. Breast Cancer Res. Treat. 72, 145–152 (2002).

86. Warren RM, Crawely A: Is breast MRI ever useful in a mammographic screening programme? Clin. Radiol. 57, 1090–1097 (2002)

87. Gorczyca DP, Sinha S, Ahn CY et al.: Silicone breast implant in vivo: MR imaging. Radiology 185, 407–410 (1992).

88. Buck A, Schirrmeister H, Kuhn T: FDG uptake in breast cancer: correlation with biological and clinical prognostic parameters. Eur. J. Nucl. Mol. Imaging 29, 1317–1323 (2002).

89. Avril N, Rose CA, Schelling M et al.: Breast imaging with positron emission tomography and fluorine-18 fluorodeoxyglucose: use and limitations.J. Clin. Oncol. 18, 3495–3502 (2000).

90. Smith IC, Welch AE, Hutcheon AW et al.: Positron emission tomography using [18F]-fluorodeoxy-D-glucose to the pathological response of breast cancer to primary chemotherapy. J. Clin. Oncol. 18, 1676–1688 (2000).

91. Schirrmeister H, Kuhn T, Guhlmann A et al.: Fluorine 18 2-deoxy-2-fluoro-Dglucose PET in the preoperative staging of breast cancer: comparison with standard staging procedures. Eur. J. Nucl. Med. 28, 351–358 (2001).

92. Tatsumi M, Cohade C, Mourtzikos KA, Fishman EK: Initial experience with FDG–PET/CT in the evaluation of breast cancer. Eur. J. Nucl. Med. Mol. Imaging 33, 254–262 (2006).

93. Sang KY, Nariya C, Woo KM: The role of PET/CT for evaluating breast cancer. Korean J. Radiol. 8, 429–437 (2007).

94. Ophir J, Alam SK, Garra B, Kallel F, Konofagou E, Krouskop T, Varghese T. 1999 Elastography: ultrasonic estimation and imaging of the elastic properties of tissues. Proc. Inst. Mech. Eng. H 213, 203–233.

95. Ophir J, Cespedes I, Ponnekanti H, Yazdi Y, Li X. 1991 Elastography: a quantitative method for imaging the elasticity of biological tissues. Ultrason. Imaging 13, 111–134

96. Konofagou E, Ophir J. 1998 A new elastographic method for estimation and imaging of lateral displacements, lateral strains, corrected axial strains and Poisson's ratios in tissues. Ultrasound Med. Biol. 24, 1183–1199.

97. Kallel F, Ophir J, Magee K, Krouskop T. 1998 Elastographic imaging of lowcontrast elastic modulus distributions in tissue. Ultrasound Med. Biol. 24, 409–425.

98. Ponnekanti H, Ophir J, Huang Y, Céspedes I. 1995 Fundamental mechanical limitations on the visualization of elasticity contrast in elastography. Ultrasound Med. Biol. 21, 533–543.

99. Thitaikumar A, Ophir J. 2007 Effect of lesion boundary conditions on axial strain elastograms: a parametric study. Ultrasound Med. Biol. 33, 1463–1467.

100. Doyley MM, Meaney PM, Bamber JC. 2000 Evaluation of an iterative reconstruction method for quantitative elastography. Phys. Med. Biol. 45, 1521.

101. Skovoroda AR, Lubinski LA, Emelianov SY, Donnell MO. 1999 Reconstructive elasticity imaging for large deformations. IEEE Trans. Ultrason. Ferroelectr. Freq. Control 46, 523–535.

102. Doyley M. 2012 Model-based elastography: a survey of approaches to the inverse elasticity problem. Phys. Med. Biol. 57, R35

103. Kallel F, Bertrand M, Ophir J. 1996 Fundamental limitations on the contrast-transfer efficiency in elastography: an analytic study. Ultrasound Med. Biol. 22, 463–470.

104. Huang SR, Lerner RM, Parker KJ. 1990 On estimating the amplitude of harmonic vibration from the Doppler spectrum of reflected signals. J. Acoust. Soc. Am. 88, 2702–2712.

105. Huang SR, Lerner RM, Parker KJ. 1992 Time domain Doppler estimators of the amplitude of vibrating targets. J. Acoust. Soc. Am. 91, 965–974.

106. Parker KJ, Huang SR, Musulin RA, Lerner RM. 1990 Tissue response to mechanical vibrations for ‘sonoelasticity imaging’. Ultrasound Med. Biol. 16, 241–246

107. Fatemi M, Greenleaf JF. 1998 Ultrasound-stimulated vibro-acoustic spectrography. Science 280, 82–85.

108. Fatemi M, Greenleaf JF. 1999 Vibro-acoustography: an imaging modality based on ultrasound-stimulated acoustic emission. Proc. Natl Acad. Sci. USA 96, 6603–6608.

109. Urban MW, Alizad A, Aquino W, Greenleaf JF, Fatemi M. 2011 A review of vibroacoustography and its applications in medicine. Curr. Med. Imaging Rev. 7, 350–359.

110. Chen S, Fatemi M, Greenleaf JF. 2004 Quantifying elasticity and viscosity from measurement of shear wave speed dispersion. J. Acoust. Soc. Am. 115, 2781–2785.

111. Chen S, Urban MW, Pislaru C, Kinnick R, Zheng Y, Yao A, Greenleaf JF. 2009 Shearwave dispersion ultrasound vibrometry (SDUV) for measuring tissue elasticity and viscosity. IEEE Trans. Ultrason. Ferroelectr. Freq. Control 56, 55–62.

112. Sandrin L, Tanter M, Gennisson JL, Catheline S, Fink M. 2002 Shear elasticity probe for soft tissues with 1-D transient elastography. IEEE Trans. Ultrason. Ferroelectr. Freq. Control 49, 436–446.

113. Sandrin L, Tanter M, Catheline S, Fink M. 2002 Shear modulus imaging with 2-D transient elastography. IEEE Trans. Ultrason. Ferroelectr. Freq. Control 49, 426–435.

114. Sarvazyan AP, Rudenko OV, Swanson SD, Fowlkes JB, Emelianov SY. 1998 Shear wave elasticity imaging: a new ultrasonic technology of medical diagnostics. Ultrasound Med. Biol. 24, 1419–1435.

115. Nightingale K, McAleavey S, Trahey G. 2003 Shear-wave generation using acoustic radiation force: in vivo and ex vivo results. Ultrasound Med. Biol. 29, 1715–1723.

116. Palmeri ML, Wang MH, Dahl JJ, Frinkley KD, Nightingale KR. 2008 Quantifying hepatic shear modulus in vivo using acoustic radiation force. Ultrasound. Med. Biol. 34, 546–558.

117. Wang M, Byram B, Palmeri M, Rouze N, Nightingale K. 2013 Imaging transverse isotropic properties of muscle by monitoring acoustic radiation force induced shear waves using a 2-D matrix ultrasound array. IEEE Trans. Med. Imaging 32, 1671–1684.

118. Rouze NC, Wang MH, Palmeri ML, Nightingale KR. 2013 Finite element modeling of impulsive excitation and shear wave propagation in an incompressible, transversely isotropic medium. J. Biomech. 46, 2761–2768.

119. Bercoff J, Tanter M, Fink M. 2004 Supersonic shear imaging: a new technique for soft tissue elasticity mapping. IEEE Trans. Ultrason. Ferroelectr. Freq. Control 51, 396–409.

120. Tanter M, Bercoff J, Athanasiou A, Deffieux T, Gennisson J-L, Montaldo G, Muller M, Tardivon A, Fink M. 2008 Quantitative assessment of breast lesion viscoelasticity: initial clinical results using supersonic shear imaging. Ultrasound Med. Biol. 34, 1373–1386

121. Li G-Y, Zheng Y, Liu Y, Destrade M, Cao Y. 2016 Elastic Cherenkov effects in transversely isotropic soft materials-I: theoretical analysis, simulations and inverse method. J. Mech. Phys. Solids 96, 388–410

122. Denis M et al. 2015 Comb-push ultrasound shear elastography of breast masses: initial results show promise. PLoS ONE 10, e0119398.

123. Mehrmohammadi M, Song P, Meixner DD, Fazzio RT, Chen S, Greenleaf JF, Fatemi M, Alizad A. 2015 Comb-push ultrasound shear elastography (CUSE) for evaluation of thyroid nodules: preliminary in vivo results. IEEE Trans. Med. Imaging 34, 97–106.

124. Song P et al. 2015 Two-dimensional shear-wave elastography on conventional ultrasound scanners with time-aligned sequential tracking (TAST) and comb-push ultrasound shear elastography (CUSE). IEEE Trans. Ultrason. Ferroelectr. Freq. Control 62, 290–302.

125. Alleyne D, Cawley P. 1991 A two-dimensional Fourier transform method for the

measurement of propagating multimode signals. J. Acoust. Soc. Am. 89, 1159–1168

126. Achenbach JD. 1973 Wave propagation in elastic solids. Amsterdam, The Netherlands: North Holland Publishing Company.

127. Yu, Y. and Acton, S.T. Speckle reducing anisotropic diffusion. *IEEE Trans. on Image Processing 11*, 11 (2002), 1260-1270.

128. Abd-Elmoniem, K.Z., Youssef, A.B.M., and Kadah, Y.M. Real-time speckle reduction and coherence enhancement in ultrasound imaging via nonlinear anisotropic diffusion. *IEEE Trans. on Biomedical Engineering 49*, 9 (2002), 997-1014.

129. Loizou, C.P., Pattichis, C.S., Christodoulou, C.I., Istepanian, R.S.H., Pantziaris, M., and Nicolaides, A. Comparative evaluation of despeckle filtering in ultrasound imaging of the carotid artery. *IEEE Trans. on Ultrasonics, Ferroelectrics and Frequency Control 52*, 10 (2005), 1653-1669.

130. Burckhardt, C.B. Speckle in ultrasound B-mode scans. *IEEE Trans. on Sonics and Ultrasonics 25*, 1 (1978), 1-6.

131. Wagner, R.F., Smith, S.W., Sandrik, J.M., and Lopez, H. Statistics of speckle in ultrasound B-scans. *IEEE Trans. on Sonics and Ultrasonics 30*, 3 (1983), 156-163.

132. Guo, Y., Cheng, H.D., Tian, J., and Zhang, Y. A novel approach to speckle reduction in ultrasound imaging. *Ultrasound in Medicine & Biology 35*, 4 (2009), 628-640.

133. Sattar, F., Floreby, L., Salomonsson, G., and Lovstrom, B. Image enhancement based on a nonlinear multiscale method. *IEEE Trans. on Image Processing 6*, 6 (1997), 888-895.

134. Gupta, S., Chauhan, R., and Sexana, S. Wavelet-based statistical approach for speckle reduction in medical ultrasound images. *Medical and Biological Engineering and Computing 42*, 2 (2004), 189-192.

135. Noble, J.A. and Boukerroui, D. Ultrasound image segmentation: A survey. *IEEE Trans. on Medical Imaging 25*, 8 (2006), 987-1010.